Long-Term Changes in Stratospheric Age Spectra in the 21st Century in the Goddard Earth Observing System Chemistry-Climate Model (GEOSCCM)

Li, Feng[1,2], Darryn W. Waugh[3], Anne R. Douglass[2], Paul A. Newman[2], Susan E. Strahan[1,2], Jun Ma[4], J. Eric Nielsen[5,2], and Qing Liang[1,2]

[1]Goddard Earth Sciences Technology and Research, Universities Research Space Association, Columbia, Maryland, USA

[2]NASA Goddard Space Flight Center, Greenbelt, Maryland, USA

[3]Johns Hopkins University, Baltimore, Maryland, USA

[4]Computational Physics Inc., Springfield, Virginia, USA

[5]Science Systems and Application Inc., Lanham, Maryland USA

Correspondence to: Feng Li (feng.li@nasa.gov)

Abstract

In this study we investigate the long-term variations in the stratospheric age spectra using simulations of the 21st century with the Goddard Earth Observing System Chemistry-Climate Model (GEOSCCM). Our purposes are to characterize the long-term changes in the age spectra and identify processes that cause the decrease of the mean age in a warming climate. Changes in the age spectra in the 21st century simulations are characterized by decreases in the modal age, the mean age, the spectral width, and the tail decay timescale. Our analyses show that the decrease in the mean age is caused by two processes: the acceleration of the residual circulation that increases the young air masses in the stratosphere, and the weakening of the recirculation that leads to the decrease of tail of the age spectra and the decrease of the old air masses. The weakening of the stratospheric recirculation is also strongly correlated with the increase of the residual circulation. One important result of this study is that the decrease of the tail of the age spectra makes an important contribution to the decrease of the main age. Long-term changes in the stratospheric isentropic mixing are investigated. Mixing increases in the subtropical lower stratosphere, but its impact on the age spectra is outweighed by the increase of the residual circulation. The impacts of the long-term changes in the age spectra on long-lived chemical traces are also investigated.

1 Introduction

Coupled Chemistry-Climate Models (CCMs) consistently simulate an acceleration of the stratospheric circulation in the recent past and the 21st century [*Butchart et al.*, 2006, 2010]. The strengthening of the stratospheric circulation in a warming climate is reflected in two diagnostics: the increase of the mean meridional mass circulation [*Butchart and Scaife*, 2001; *Butchart et al.*, 2006, 2010; *Li et al.*, 2008; *Garcia and Randel*, 2008; *McLandress and Shepherd*, 2009] and the decrease of the mean age of stratospheric air [*Austin and Li*, 2006; *Oman et al.*, 2009; *Butchart et al.*, 2010]. These two diagnostics are strongly correlated [*Austin and Li*, 2006], but they have different physical meanings. The mean meridional mass circulation, often approximated by the Transformed Eulerian Mean residual circulation, represents the mean advection part of the stratospheric transport circulation [*Andrews et al.*, 1987]. In this paper the mean meridional mass circulation is referred as the residual circulation, although in other literatures it is also called the Brewer-Dobson circulation or diabatic circulation [e.g., *Andrews et al.*, 1987; *Shepherd*, 2002]. The mean age of air is the average time for an air parcel to transport from troposphere to a stratospheric sample region. It is a measure of the strength of the stratospheric transport circulation. The mean age is determined not only by the residual circulation, but also by other processes such as isentropic mixing and recirculation [*Waugh and Hall*, 2002].

There are very few observational studies to verify the simulated mean age changes. *Engel et al.* [2009] examined a long-term record of mean age of air derived from CO_2 and

60 SF_6 measurements in the northern midlatitudes and found no significant trend in the last
61 three decades, contrary to CCM simulations. However, *Garcia et al.* [2011] pointed out
62 that the results of *Engel et al.* [2009] have serious caveats due to sparse sampling and the
63 nonlinear growth rate of CO_2 and SF_6. Nevertheless, there are still doubts on the model
64 projected mean age changes.
65
66 A major concern of the model results is that the mechanism for the decrease of the mean
67 age is not clear. Previous studies have shown that the increase of the residual circulation
68 plays an important role in driving the trend of the mean age [*Austin and Li*, 2006; *Garcia*
69 *et al.*, 2007; *Oman et al.*, 2009], but there is not a complete understanding how these two
70 processes are related. *Strahan et al.* [2009] demonstrated that in the tropical pipe the
71 timescale of the residual circulation is significantly smaller than the mean age. The
72 differences between the two timescales are caused by recirculation of air parcels between
73 the tropics and midlatitudes. An air parcel could make multiple circulates between the
74 tropics and midlatitudes. This recirculation process depends on mixing through the
75 subtropical transport barriers [*Neu and Plumb*, 1999]. Thus changes in recirculation and
76 mixing could also impact the trend of the mean age. But it is not clear how recirculation
77 and mixing respond to greenhouse gas increases and how these changes impact the mean
78 age.
79
80 Investigating the long-term changes in the age spectra will help to clarify the roles of
81 changes in the residual circulation, recirculation and mixing in driving the decrease of the
82 mean age. The age spectrum is the probability distribution function of transit times

between a source region in the troposphere or tropopause and a sample region in the stratosphere [*Hall and Plumb*, 1994; *Waugh and Hall*, 2002]. The mean age is the first moment of the age spectrum, or the average of all the possible transit times. In addition to the mean age, other important parameters that characterize the age spectrum include the modal age and spectral width. The modal age corresponds to the time of the spectral peak. It represents the most probable transit time and is directly associated with the timescale of the bulk velocity of tracer transport [*Waugh and Hall*, 2002]. The modal age agrees very well with the timescale of the residual vertical velocity within the tropical pipe region [*Strahan et al.*, 2009]. The spectral width is related to the second moment of the age spectrum and is a measure of the strength of the recirculation [*Strahan et al.*, 2009]. The age spectrum contains complete information on transit times and is more useful than the mean age in understanding the distribution of photochemically important trace species in the stratosphere [*Schoeberl et al.*, 2005; *Waugh et al.*, 2007]. While the decrease of the mean age in the 21st century has been extensively documented, no previous studies have investigated the long-term changes in the age spectra.

In this paper we investigate the long-term changes in the stratospheric age spectra in the 21st century using simulations with the Goddard Earth Observing System Chemistry-Climate Model (GEOSCCM). The main purposes of this study are to characterize the long-term changes in the age spectra and to identify processes that cause the decrease of the mean age. This paper is organized as following. A brief review of the age spectrum theory and a detailed description of our method to calculate the age spectra are given in Section 2. This is followed by an introduction of the GEOSCCM and the experiment

106 setup in Section 3. Results are presented in Section 4. Discussions are given in Section
107 5. Section 6 is the conclusion.
108
109 ## 2 Method
110
111 The age spectrum is a Green's function, or a boundary propagator, that solves the
112 continuity equation for the mixing ratio of a conserved and passive tracer [*Hall and*
113 *Plumb*, 1994]. It is also called the Transit-Time Distribution (TTD) in ocean and
114 tropospheric transport literatures [*Holzer et al.*, 2003; *Haine et al.*, 2008]. The age
115 spectrum is expressed by

116 $$\chi(r,t) = \int_0^\infty \chi(\Omega, t-\xi) G(r,t \mid \Omega, t-\xi) d\xi \qquad (1)$$

117 where $\chi(r,t)$ is the tracer mixing ratio at a sample region r and sample time t, ξ is the
118 elapse of time between the sample time t and source time t′ (i.e., $\xi = t - t'$), the source time
119 t′ is when the tracer had last contact with the boundary resource region Ω , and $G(r,t|\Omega,t-\xi)$
120 ξ) is the age spectrum. The physical meaning of the age spectrum is clear in Equations 1:
121 $G(r,t|\Omega,t-\xi)d\xi$ represents the mass fraction of the air parcel at r and t that was last in
122 contact with Ω between ξ and $\xi+d\xi$ ago.
123
124 Different methods have been used to calculate age spectra [e.g., *Hall and Plumb*, 1994;
125 *Schoeberl et al.*, 2003; *Haine et al.*, 2008]. Among all the methods that have been used,
126 the pulse tracer method is the most direct approach. It should be emphasized that the
127 pulse tracer method does not directly produce the age spectrum. Instead it generates
128 another kind of boundary propagator $G(r,t'+\xi|\Omega, t')$, which is called the Boundary

129 Impulse Response (BIR) [*Haine et al.*, 2008; *Li et al.*, 2012]. Once the BIR is obtained,
130 the age spectrum can be calculated from the BIR.
131
132 Replace t with t′+ξ, then Equation 1 becomes
133 $$\chi(r,t'+\xi)=\int_0^\infty \chi(\Omega,t')G(r,t'+\xi\,|\,\Omega,t')d\xi \qquad (2)$$
134 Note that if we set the boundary condition of $\chi(\Omega,t')$ as a Dirac delta function, then
135 Equation 2 yields $\chi(r,t'+\xi) = G(r,t'+\xi|\Omega,t')$. Thus the BIR is the time evolving response
136 to a delta function boundary condition. The BIR can be easily calculated in models using
137 the pulse tracer: release a pulse of a conserved and passive tracer at a chosen source
138 region and source time, and the time series of the tracer's mixing ratio at any interior
139 point *r* is $G(r,t'+\xi|\Omega, t')$.
140
141 The mathematic relationship between the BIR and the age spectrum is simple, but
142 Equation 2 does not have the same clear physical meaning as Equation 1. It is important
143 to recognize that the age spectrum and the BIR are different due to their time dependence.
144 Only in the special case of steady flow the age spectrum is the same as the BIR. In this
145 case we calculate a single realization of the BIR as the age spectrum [*Haine et al.*, 2008].
146 Computing the age spectrum in unsteady flow is more complicated and requires a series
147 of BIRs that are launched in different source times [*Holzer et al.*, 2003; *Haine et al.*,
148 2008; *Li et al.*, 2012]. There are two approaches. If one is interested in the seasonal and
149 interannual variability of the age spectra, then one needs to reconstruct time varying age
150 spectra from BIRs [*Li et al.*, 2012]. But if one is mainly interested in the time-averaged
151 properties of the age spectra, one can use the mean of an ensemble of BIRs as a time-

averaged age spectrum. This is because the BIR and the age spectrum share the same boundary propagator distribution (*Haine et al.* [2008]).

The stratospheric transport has large seasonal and interannual variations. These variabilities have to be accounted for in order to correctly capture the annual mean or the seasonal properties of the age spectra. *Li et al.* [2012] investigated the seasonal variations of the stratospheric age spectra in the GEOSCCM. They reconstructed seasonally varying age spectra from twelve BIRs released in each month of the annual cycle. Here, we focus on the long-term changes in the time-averaged properties of the age spectra, and take the second approach introduced above to use the mean of an ensemble of BIRs launched in different times as the time-averaged age spectra.

The method of *Hall et al.* [1999b] is followed to conduct the pulse tracer experiment. The tropical lower troposphere between 10°N and 10°S and from the surface to about 800 hPa is chosen to be the boundary source region. As an approximation of the delta function boundary condition, the mixing ratio of the tracer is set to an arbitrary positive value in the first month of the experiment and then held as zero through the rest of the experiment in the boundary source region. There are no other sources or sinks for the tracer. The pulse experiment runs for 20 years.

We perform an ensemble of ten pulse tracer experiments in a 20-year period and use the mean of the resultant ten BIRs as the time-averaged age spectra in this period. The ten pulse tracers are released respectively in January and July in each of the first five years of

175 the 20-year period. The different release times of the pulse tracers are chosen to
176 represent the seasonal and interannual variability of stratospheric transport. We conduct
177 these ten pulse tracer experiments for each of the five 20-year periods in a 21st century
178 simulation with the GEOSCCM. A total of fifty BIRs are calculated and five age spectra
179 are obtained. The five age spectra cover the model year 2000-2019, 2020-2039, 2040-
180 2059, 2060-2079, and 2080-2099, respectively.
181
182 Figure 1 shows examples of the BIRs and their ensemble mean in 3 different locations in
183 the 2000-2019 period. The BIRs released in January and July are shown in red and blue,
184 respectively. The BIRs have strong seasonal and interannual variability. In the tropics,
185 the interannual variability reflects the impacts of the quasi-biennial oscillation (QBO) on
186 the BIRs. In the extratropics, seasonal differences of the BIRs stand out, although there
187 are considerable interannual variations. The age spectrum (thick black line), i.e. the
188 ensemble mean of the BIRs, is different from the ensemble members. Therefore it is
189 important to use an ensemble of BIRs in order to accurately capture the time-averaged
190 property of the age spectra.
191
192 **3 GEOSCCM and Simulation**
193
194 The model we use in this study, the GEOSCCM [*Pawson et al.*, 2008], couples the
195 GEOS5-AGCM [*Rienecker et al.*, 2008] with a comprehensive stratospheric chemistry
196 package [*Douglass et al.*, 1997]. The GEOSCCM has 72 vertical levels with a model top
197 at 0.01hPa. The horizontal resolution in the GEOSCCM is adjustable and a grid of 2°

198 latitude by 2.5° longitude is used in this study. The pulse tracer experiments were carried
199 out with a sensitivity simulation of the 21st century in which CO_2 increases under the
200 IPCC (2001) A1b scenario, but the amount of ozone depleting substances (ODSs) and
201 other greenhouse gases are fixed at the year 2000 level conditions. The simulation uses
202 modeled sea surface temperature and sea ice in the 21st century under the A1b scenario
203 from the NCAR Community Climate System Model 3.0. In this sensitivity simulation,
204 the model climate change is solely driven by increases in CO_2 and sea surface
205 temperature. As described in detail in the previous section, a total of fifty pulse tracer
206 experiments are carried out with the simulation. Fifty BIRs are generated and five age
207 spectra are computed. In the rest of the paper, the five age spectra are referred as 2000,
208 2020, 2040, 2060, and 2080 spectra, respectively. All results presented in this paper are
209 zonally and monthly averaged.
210
211 The GEOSCCM has participated in the Chemistry-Climate Model Validation Activity 2
212 (CCMVal-2) and is one of the best models in CCMVal-2 [*SPARC CCMVal*, 2010].
213 GEOSCCM simulations of the recent past compare well with observations in
214 stratospheric chemistry, transport, and dynamics [*SPARC CCMVal*, 2010; *Strahan et al.*,
215 2011]. Quite realistic stratospheric transport characteristics, such as the mean age, the
216 tropical ascent rate, and the lower stratospheric mixing rate, are captured by the
217 GEOSCCM. But the Antarctic polar vortex is more isolated in GEOSCCM than
218 observed, a common bias in CCMs. The version of the GEOSCCM used in this study is
219 slightly different from the one participated in CCMVal-2 in that it produces a QBO by
220 increasing the non-orographic gravity wave source in the tropics.

221

222 **4 Results**

223

224 Our simulation projects a decrease in the mean age of air and an increase in the residual
225 circulation in the 21st century, consistent with previous CCM studies [e.g., *Butchart et*
226 *al.*, 2006, 2010]. Figure 2a shows the differences in the mean age of air between the
227 2080 and 2000 spectra, where the mean age is computed from the age spectrum by
228 $\Gamma(r,t) = \int_0^\infty \xi G(r,t \mid \Omega, t-\xi) d\xi$. The mean age is younger in 2080 than in 2000
229 everywhere in the stratosphere. The rate of decrease is larger in the midlatitudes than in
230 the tropics, indicating a reduced mean age gradient between these two regions and an
231 enhanced tropical ascent rate [*Neu and Plumb*, 1999]. Strong decrease in the mean age is
232 found in the subtropical and midlatitude lower stratosphere in both hemispheres,
233 suggesting an increase of the quasi-horizontal transport in this region. In the northern
234 hemisphere lower stratosphere the area of large mean age decrease extends to the high
235 latitudes. The largest decrease in the mean age is found in the Arctic lower stratosphere
236 (over 0.8 years, or 20%). This suggests the acceleration of the quasi-horizontal transport
237 is particularly strong in the northern hemisphere. Overall these results agree well with
238 those produced by the version of the GEOSCCM that participates in CCMVal-2
239 [*Butchart et al., 2010*], although the decrease of the mean age is larger in the current
240 simulation. Note that in CCMVal-2 the GEOSCCM simulates ozone recovery in the 21st
241 century. A stronger decrease in the mean age without ozone recovery is consistent with
242 the findings of *Oman et al.* [2009] that ozone recovery in the 21st century acts to reduce
243 the rate of mean age decrease.

244

245 The decrease in the mean age of air is consistent with the acceleration of the residual
246 circulation (Figures 2b and 2c). The changes in the residual vertical velocity ($\overline{w}^*$) and
247 meridional velocity ($\overline{v}^*$) clearly show two cells in each hemisphere. The increase in the
248 residual velocities is much stronger in the lower and upper stratosphere than in the middle
249 stratosphere. Within each cell increase in the tropical upwelling is balanced by increase
250 in the poleward mass transport and extratropical downwelling. Changes in the lower
251 branch of the residual circulation are confined to the tropics and midlatitudes, whereas
252 the increase of the upper branch of the residual circulation extends all the way to the high
253 latitudes.

254

255 Previous studies have shown that the mean age is strongly correlated with the tropical
256 upward mass flux in the lower stratosphere, a measure of the overall strength of the
257 residual circulation [*Austin and Li*, 2006; *Butchart et al.*, 2010]. But the timescale of the
258 residual circulation should not be confused with the mean age. The residual velocity
259 approximates the bulk velocity of tracer transport. *Waugh and Hall* [2002] showed that
260 the timescale of the residual circulation (or bulk tracer transport) is closely associated
261 with the modal age in regions of weak mixing such as the tropical pipe. The modal age
262 and the timescale of the residual circulation are smaller than the mean age because the
263 stratospheric age spectrum has an asymmetric shape with a long tail [*Hall and Plumb*,
264 1994]. *Schoeberl et al.* [2008] calculated the vertical velocity for water vapor advection
265 from the tape recorder signal in the tropical pipe and found that it agrees very well with
266 the residual vertical velocity. *Strahan et al.* [2009] further showed that the modal age is a

lower limit of the timescale of the residual vertical velocity and both are shorter than the mean age.

In order to illustrate the relationship between the mean age, the modal age, and the timescale of the residual circulation, Figure 3 compares these three timescales in the tropical pipe region between 10°N and 10°S and from 70 hPa to 1 hPa. First we note that the transit time of the mean vertical advection is closely associated with the modal age and is significantly shorter than the mean age (Figure 3a), confirming the results of *Strahan et al.* [2009]. The mean age, modal age, and the timescale of the vertical advection are all shorter in 2080-2099 than in 2000-2019 (Figure 3b). The decreases in the vertical advection timescale and modal age are comparable to each other in most of the stratosphere, and they are distinctly smaller than the decrease of the mean age. In terms of the absolute value, decreases in the mean age are more than twice those in the transit time of the vertical advection. The relative changes in the mean age are also larger than that in the transit time of the vertical advection. This example shows that the decrease of the mean age can only be partly explained by the acceleration of the residual velocities.

Although the decrease in the mean age in a warming climate has been well documented [*Garcia* and *Randel*, 2009; *Oman et al.*, 2009], no previous studies have investigated the long-term changes in other important age spectral parameters such as the modal age and width. Figure 4 shows the distribution of the modal age and spectral width of the 2000 spectra (contour) and the differences between the 2080 and 2000 spectra (color). The

distribution of the modal age is somewhat similar to the mean age, but the modal age has strong gradients in the high latitude lower stratosphere. The modal age increases by up to 2-4 times in a very narrow latitudinal band in this region. From 2000 to 2080 the modal age decreases in most of the stratosphere. The changes in the modal age are less smoothly distributed than the changes in the mean age. In general the decrease in the modal is smaller in the tropics than in the high latitudes. The largest decrease is seen in the polar lower stratosphere, especially in the Arctic. We will show later that the large change of the modal age in the polar lower stratosphere is caused by change in the multi-mode spectral shape in this region.

The spectral width is related to the square root of the second moment of the age spectrum by $\Delta(r,t) = \sqrt{\frac{1}{2}\int_0^\infty (\xi - \Gamma(r,t))^2 G(r,t \mid \Omega, t-\xi) d\xi}$. It quantifies the spread of the transit time distribution [*Waugh and Hall,* 2002]. Qualitatively, the width indicates how important the tail of the spectrum contributes to the mean age. The wider the width, the longer the tail, and the larger the fraction of the tail contributes to the mean age. The tail of the age spectrum is related to the strength of the recirculation, thus the width can also be viewed as a measure of the strength of the recirculation [*Strahan et al.*, 2009]. Figure 4b shows that the distribution of the spectral width is similar to that in the mean age below about 10 hPa, but the width becomes uniform with a value of about 2 years above 10 hPa. Throughout the stratosphere, the spectral width becomes narrower at 2080 than at 2000. The largest decreases in the width are found in the subtropical (20°-40° N and S) lower stratosphere.

313 We now examine the distribution of the age spectra and their changes at 50 and 10 hPa.
314 The focus is on the lower stratosphere because the largest changes in the mean age,
315 modal age, and spectral width occur below 10 hPa. Figure 5 shows the 2000 age spectra
316 at 50 hPa as a function of latitude and the differences between the 2080 and 2000 age
317 spectra. The age spectra have an asymmetrical shape with a young peak and a long tail.
318 Only the first 10 years of the age spectra are shown because the tail of the spectra decays
319 rapidly with increasing transit time. The age spectra have large latitudinal variations with
320 younger and stronger peaks and more compacted distribution in the tropics than in the
321 extratropics. The modal age has very sharp gradients around 70° latitudes in both
322 hemispheres with values increasing by more than 2 times in a narrow latitudinal band.
323
324 The 2080 age spectra have higher percentages of young air and lower percentages of old
325 air compared to the 2000 age spectra (Figure 5b). The transition from positive (more
326 young air) and negative (less old air) differences follows approximately the modal age of
327 the 2000 age spectra. This indicates that the spectral peaks become younger and stronger
328 in the 2080 spectra. These changes lead to decreases in the mean age and spectral width.
329 Furthermore, a younger and stronger spectral peak together with a narrower width means
330 that the 2080 age spectra have a shorter tail. There are multiple peaks at high latitudes,
331 suggesting the age spectra in this region have a multi-model shape [*Li et al.*, 2012].
332
333 Overall the age spectra at 10 hPa are similar to those at 50 hPa, although they have
334 smaller latitudinal variations, especially in the spectral width (Figure 6a). The changes
335 between the 2080 and 2000 age spectra at 10 hPa are also similar to those at 50 hPa

(Figure 6b). Again the 2080 spectral have a larger fraction of young air than the 2000 age spectra and the change from more young air to less old air occurs at about the time of the modal age of the 2000 spectra. A notable discrepancy is that the age spectra differences at high latitudes at 10 hPa do not show multiple peaks.

We investigate the changes in age spectra in the lower stratosphere in more detail by examining the evolution of the age spectra at 50 hPa in different locations. Figure 7 clearly shows that as the integration progresses, the modal ages become younger, the spectral peaks get stronger, the tails are shorter, and the widths are narrower. The age spectra undergo larger changes in 2020-2039 than in other periods. The age spectra at high latitudes, particularly in the Arctic, have different characteristics from those at low and middle latitudes. They have multiple peaks with comparable magnitude, in contrast to the single-mode shape at lower latitudes. For example, in the Arctic the 2000 spectrum (black line) has 3 peaks between 3 and 4 years of transit time (Figure 7e). The strongest peak, which is just slightly stronger than other peaks, occurs at 3.7 years. This multi-mode spectral shape indicates that there are multiple, nearly equally important transport pathways to the polar lower stratosphere. From 2000 to 2080, the percentages of air younger than 2 years increase significantly from 15% to 25%. The percentages of air with transit time between 2 and 4 year increase only slightly from 36% to 38%. The fraction of air older than 4 years decreases from 49% in 2000 to 37% in 2080. In the 2080 spectrum (red line) the peak at 1.8 years becomes the strongest among several comparable peaks, and we obtain a decrease of modal age of 1.9 years from 2000 to 2080. However, the spectral peak at 1.8 years in the 2080 spectrum does not correspond

359 to the peak at 3.7 years in the 2000 spectrum. The dramatic modal age change reflects
360 the changes of relative strength of the multiple peaks.
361
362 The results presented in Figures 5-7 indicate that the decrease of the mean age in the
363 2080 age spectra is due to an increases in the percentage of the young air and a decrease
364 in the percentages of the old air, or the tail of the age spectra. The changes in the tail of
365 the age spectra can be more easily seen when the age spectra are plotted in the
366 logarithmic scale. Figure 8 is the same as Figure 7, but it uses the logarithmic scale and
367 covers the whole 20-year period. There are several interesting features regarding the
368 distribution and change of the tail of the age spectra. First, the tail can be represented by
369 a linear regression line. That is, the tail is approximated very well by an exponentially
370 decaying mode $\Psi_0(r,t)\exp(-\frac{\xi}{\tau_0})$, where τ_o is the decay timescale. Second, the slope of
371 the tail, or the decay timescale τ_o, appears to be independent of locations. And third, the
372 tails are shorter in 2080 than in 2000. The decrease in the tail can be quantified by a
373 decrease in τ_o.
374
375 The decay timescale τ_o has long been known as a fundamental stratospheric transport
376 diagnostic [*Prather* 1996; *Hall et al.*, 1999a; *Ehhalt et al.*, 2004]. Under the steady state
377 condition, the age spectrum can be decomposed into a set of normal modes, each of
378 which decays exponentially at a timescale that is equal to the reverse of its eigenvalue
379 [*Hall et al.*, 1999a]. The base mode has the longest decay timescale τ_o and it decays
380 more slowly than the higher modes. For long transit time, only the base mode survives
381 and thus the tail of the age spectrum can be approximated by the base mode. τ_o is a

382 unique transport diagnostic because it is independent of location. Physically τ_o describes
383 how fast the mixing ratio of a conserver tracer in the stratosphere decays due to transport
384 alone [*Ehhalt et al.*, 2004]. It can also be viewed as an integrated measure of the strength
385 of stratospheric recirculation.
386
387 The decrease in the mean age of air through the 21st century is strongly correlated with
388 the decrease of τ_o. Figure 9a plots the evolution of τ_o from 2000 to 2080 against the
389 globally and stratospherically (100-1 hPa) averaged mean age. When calculating τ_o, the
390 tail of the age spectra is regressed onto a single exponentially decay mode. Here we
391 define the tail as the region with transit time older than 4 years, noting that the age
392 spectra start to exponentially decay at about 4 years (see Figure 8). The correlation
393 between τ_o and the mean age is 0.998, though we only have 5 samples. This strong
394 correlation indicates that the decrease of the tail makes a significant contribution to the
395 decrease of the mean age.
396
397 The decrease of τ_o is highly anti-correlated with the increase of the upward mass flux in
398 the tropical lower stratosphere (Figure 9b), which means that an accelerated residual
399 circulation acts to weaken the stratospheric recirculation. It is known that changes in
400 mixing cross transport barriers could affect recirculation [*Neu and Plumb*, 1999; *Strahan*
401 *et al.*, 2009], but our results show that the stratospheric mean meridional circulation has a
402 significant impact on recirculation and the tail part of the age spectra (also see
403 discussions in Section 5.1).
404

405 The tail of the age spectra has received less attention than other spectral parameters in
406 previous studies, but the tail has a significant impact on the mean age [*Schoeberl,* 2003,
407 2005]. The mean age can be regarded as the mixing ratio of an ideal clock tracer that has
408 a linearly increasing stratospheric source and a fixed tropospheric concentration [*Waugh*
409 *and Hall*, 2002]. Therefore the tail of the age spectra weights heavily on the mean age.
410 Figure 10a shows the fractional contribution of the tail (defined as transit times old than 4
411 years) to the mean age in the 2000 spectra (contour) and the changes of the fractional
412 contribution between the 2080 and 2000 spectra (color). The distributions of the tail
413 contribution look similar to those of the mean age. The tail contributes a small fraction to
414 the mean age in the tropical lower stratosphere where the age spectra are dominated by
415 young spectral peaks. In the rest of the stratosphere, however, the tail accounts for more
416 than 50% of the mean age. From 2000 to 2080, the tail becomes shorter and its fractional
417 contributions to the mean age decrease everywhere in the stratosphere. The largest
418 decrease of the tail contribution occurs in the subtropical lower stratosphere between 20°
419 and 30° latitudes and centered at 70 hPa, which corresponds to the largest decrease in the
420 spectral width (see Figure 4b). This correspondence is not a complete surprise as the
421 width is closely linked with the tail.
422
423 The changes in the tail can also be quantified by the changes in the averaged transit time
424 in the tail, referred to as the tail age here. Comparing Figure 10b with Figure 2a reveals
425 that the tail age decreases more than the mean age between 2080 and 2000. This
426 confirms that the decrease in the tail decay timescale indeed makes an important
427 contribution to the decrease in the mean age. The differences between changes in the

mean age and tail age are those from air younger than 4 years. It can be inferred from Figure 10b and Figure 2a that the average transit time for air parcels younger than 4 years is shorter at 2080 than at 2000.

5 Discussions

5.1 Long-Term Changes in Isentropic Mixing

In addition to the residual circulation, changes in isentropic mixing could also impact the trend of the mean age and age spectra. For instance, enhanced mixing from the midlatitudes to the tropics increases the probability of recirculation within the stratosphere, and thus leads to a longer tail, a wider width, and an older mean age [*Neu and Plumb*, 1999; *Strahan et al.*, 2009]. However, it is not clear how stratospheric mixing changes in the 21st century, and what are the impacts of the changes in mixing on the age spectra. Here we calculate the equivalent length of N_2O to investigate the long-term changes in isentropic mixing. The equivalent length of a chemical tracer measures the geometry complexity of the tracer contours in the equivalent latitude coordinate on isentropic surfaces [*Nakamura*, 1996; *Ma et al.*, 2003]. *Nakamura* [1996] showed that the equivalent length, or more accurately its square, is a useful diagnostic of the efficiency of isentropic tracer mixing.

Figure 11 shows the distribution of the normalized equivalent length squared of N_2O (η) for 2000-2019 (lines) and the relative differences between 2080-2099 and 2000-2019 (colors). Large values of η correspond to strong mixing, whereas small values indicate

451 weak mixing, or transport barrier. The subtropical barrier, polar vortex barrier, and
452 extratropical surf zone can be recognized in Figure 11. The base of the tropical pipe,
453 identified by strong gradient in η in the tropical lower stratosphere, has a "V" shape.
454 Large values of η are also found in the tropical/subtropical lower stratosphere,
455 corresponding to the so-called "tropically controlled transition region". In order to test
456 the robustness of these results, we also calculate the equivalent length using CH_4 and find
457 almost exactly same results (not shown). This gives us confidence in using the
458 equivalent length to diagnose changes in stratospheric mixing.
459
460 The most striking feature in the changes of η between 2080-2099 and 2000-2019 is a
461 large increase in η in the tropical/subtropical lower stratosphere. Mixing increases up to
462 50% in the base of the tropical pipe. There are essentially no changes in mixing across
463 the subtropical barriers in the middle and upper stratosphere. Thus the tropical pipe
464 becomes more leaky, but only in the base. Mixing decreases significantly just below the
465 tropical pipe and the area of reduced η extends to midlatitudes. Mixing increases in the
466 Arctic lower stratosphere, but it remains the same in the Antarctic stratosphere.
467
468 The pattern of changes in η in the tropical/subtropical lower stratosphere indicates that
469 the distribution of η is shifted upward in this region from 2000-2019 to 2080-2099. The
470 upward shift in the mixing pattern is consistent with the zonal wind changes. Figure 12
471 shows the changes in temperature and zonal wind between 2080-2099 and 2000-2019.
472 The meridional temperature gradient increases in the subtropical upper troposphere and
473 lower stratosphere (UTLS), due to strong warming in the tropical upper troposphere.

474 This causes significant westerly acceleration of the zonal wind in the tropical/subtropical
475 UTLS, leading to an upward lift of the subtropical jets and the zero wind line. *Shepherd*
476 *and McLandress* [2011] showed that, through critical-layer control, the upward lift of the
477 zonal wind in the subtropical lower stratosphere shifts higher the wave breaking altitude,
478 which drives the acceleration of the lower branch of the residual circulation. Since
479 mixing is generated by wave breaking, we argue that the upward shift of wave breaking
480 could also explain changes in mixing in the tropical/subtropical lower stratosphere.
481
482 In order to demonstrate the relationship among changes in isentropic mixing, residual
483 circulation, and zonal wind, Figure 13a plots the evolution of the 20-year mean η
484 averaged in 10°-30° latitudes and 440-520 K against the tropical upward mass flux at 70
485 hPa and the subtropical UTLS zonal wind averaged in 10°-30° latitudes and 200-70 hPa
486 in bother hemispheres. The strong correlations among the three diagnostics support our
487 argument that the increases in the mixing and residual circulation are closely related to
488 each other, and both are driven by zonal wind changes that lead to enhanced wave
489 breaking in the subtropical lower stratosphere.
490
491 However, the increase in mixing in the subtropical lower stratosphere does not produce
492 older main age or wider width in this region. Figure 13b shows that as mixing increases,
493 the mean age (black line) and the spectral width (blue line) in the subtropical lower
494 stratosphere decrease. *Ray et al.* [2010] showed that, using the conceptual tropical leaky
495 pipe model, the trend of the mean age is very sensitive to the relative importance of
496 changes in the upwelling and mixing. One important result in this study is that changes

497 in mixing and upwelling are not independent to each other; rather they are closely related.
498 Our model results indicate that the impact of enhanced mixing on the age spectra is
499 outweighed by the acceleration of the residual circulation.
500
501 **5.2 Relationship between Changes in Age Spectra and Chemical Tracers**
502
503 The mean age of air is compactly related with long-lived chemical tracers such as N_2O
504 and CH_4 in the lower stratosphere [e.g., *Boering et al.*, 1996]. This compact relationship
505 can be used to infer the distribution of the mean age. For example, *Andrews et al.* [2001]
506 derived an empirical relationship between the mean age and N_2O in the midlatitude lower
507 stratosphere from NASA ER-2 aircraft measurements. Applying this relationship to all
508 latitudes, they estimated the seasonal distribution of the mean age in the lower
509 stratosphere. However, as the mean age and age spectra change in response to CO_2
510 increases in the 21st century, the relationship between the mean age and chemical tracers
511 also changes.
512
513 Figure 14a compares the compact relationship between the mean age and N_2O in 2000-
514 2019 and 2080-2099 in the northern hemisphere lower stratosphere 100-50 hPa. For age
515 older than about 1.5 years, the compact line in 2080-2099 is shifted to the left of the line
516 in 2000-2019. This shift means that the mean age and N_2O respond differently to
517 circulation change in the 21st century. As the residual circulation speeds up, the
518 distribution of the mean age and long-lived chemical tracers are lifted upward, but the

519 upward lifting in the mean age is stronger such that a given mean age is associated with a
520 smaller mixing ratio of N_2O in 2080-2099 than in 2000-2019.
521
522 The mean age also exhibits a compact relationship with fractional release of
523 chlorofluorocarbons (CFCs) [*Shauffler et al.*, 2003]. The fractional release is defined as
524 $fr = 1 - \chi(r)/\chi_0$, where $\chi(r)$ is the mixing ratio of a CFC at a stratospheric sample region r,
525 and χ_0 is the mixing ratio of the same CFC that would have had if there was no chemical
526 loss [*Shauffler et al.*, 2003]. The fractional release provides useful information on
527 photochemical loss of CFCs. Figure 14b shows that the compact relationship between
528 the mean age and CFC12 (CF_2Cl_2) changes from 2000-2019 to 2080-2099 in a manner
529 similar to the change of the mean age – N_2O relationship. Note that when calculating the
530 fractional release, χ_0 is simply taken as the fixed boundary condition value. But in
531 general when the boundary condition changes with time, χ_0 is calculated using Equation 1
532 with the knowledge of the age spectrum.
533
534 Our results are very similar to *Douglass et al.* [2008], who also showed that the
535 GEOSCCM reproduces the observed compact relationship between the mean age and the
536 fractional release. The shift in the relationship between the mean age and the long-lived
537 tracers indicates that the mean age is more sensitive to the circulation change than the
538 tracers. We argue that this is because the tracers are less sensitive to change in the tail of
539 the age spectra. As discussed in the previous section, changes in the tail of the age
540 spectra significantly impact the mean age (see Figure 10). The chemical tracers,
541 however, are not as sensitive to the tail of the age spectra [*Schoeberl et al.*, 2005]. The

542 air parcels in the tail region could have released most of the chemical tracer they carry
543 because they are likely to experience higher maximum altitude and stronger
544 photochemical loss than those has shorter transient times [*Waugh et al.*, 2007; *Douglass*
545 *et al.*, 2008]. Therefore chemical tracers respond differently to changes in the age
546 spectra.
547
548 We use the ideal "radioactive" tracer to test the above hypothesis. Assume the
549 radioactive tracer has a spatially uniform decay rate λ in the stratosphere and a fixed
550 surface concentration c, its mixing ratio can be written as

551 $$\chi(r,t) = c\int_0^\infty e^{-\lambda\xi} G(r,t \mid \Omega, t-\xi)d\xi . \qquad (3)$$

552 [*Schoeberl et al.*, 2005]. In contrary to the clock tracer, the mixing ratio of the
553 radioactive tracer relies more on the head than the tail of the age spectrum. Since we
554 have the age spectrum, we can calculate the mixing ratio and the mass burden of the
555 radioactive tracer from Equation 3. Figure 15 shows the evolution of the stratospheric
556 (100-1 hPa) mass burden of three radioactive tracers with different decay rate. For
557 comparison the evolution of the stratospheric burden of CFC11 (green), CFC12 (blue)
558 and the mean age (dashed) are also plotted. Except for the mean age, all other tracers'
559 stratospheric burden increases in the 21st century. For the radioactive tracers, the faster
560 the decay rate the larger the mass burden increasing. The mass burden of CFC11
561 increases more than that of the CFC12.
562
563 To better understand the different long-term changes of the mass burden of these tracers,
564 we calculate the changes of stratospheric air masses as a function of transit time. Figure

16a shows the air mass changes between 2080 and 2000 normalized to the total stratospheric air mass burden, and Figure 16b is the relative changes between 2080 and 2000. The stratospheric air mass burden is a constant, but the distribution of air masses changes with time. The air masses younger than 2 years increase and the air masses older than 2 years decrease between 2080 and 2000. The changes of the young and old air masses compensate each other. However, the mass burden of tracers may increase or decrease with time depending on how the tracers weight toward different parts of the age spectrum. The mean age, i.e., the mixing ratio of the clock tracer, decreases because the clock tracer weights more in the old air than the young air. The radioactive tracers are more sensitive to the changes in the young air than the old air, and the mass burden of the radioactive tracers increases. A radioactive tracer with a faster decay rate has a larger weighting in the young air masses than one with a slower decay rate, and therefore its stratospheric mass increases more. This argument can be used to explain different changes in CFC11 and CFC12. CFC11 has a stronger local chemical loss frequency than CFC12 [*Douglass et al.*, 2008], and its stratospheric mass burden increases more than CFC12. Note that all the above arguments are based on the condition that the tracer's surface boundary condition is fixed. Nevertheless, our analyses clear show that the age spectrum is more relevant to chemical tracers than the mean age.

6 Conclusion

The long-term changes in the stratospheric age spectra in response to CO_2 increases in the 21st century are investigated using the GEOSCCM simulations. Changes in age spectra

588 are characterized by increases in young air masses and decreases in old air masses,
589 younger and stronger peaks, shorter tails, and more compacted distribution. These
590 changes lead to decreases in the mean age, modal age, spectral width, and tail decay
591 timescale. An important result of this study is that changes in the tail of the age spectra
592 make an important contribution to the decrease in the mean age.
593
594 A major purpose of this paper is to identify processes that cause the long-term changes in
595 the mean age of air. Our analyses show that the decrease in the mean age is driven by
596 two processes. The first process is the acceleration of the residual circulation that
597 increases young air masses in the stratosphere. This process has been shown to be
598 directly associated with the decrease of the modal age in the tropical pipe region. The
599 second process is the weakening of the recirculation in the stratosphere, which leads to a
600 shorter tail of the age spectra and a decrease of old air masses. This process is quantified
601 by the decrease in the decay timescale of the tail of the spectra. We have shown that the
602 decrease in the tail decay timescale is strongly correlated with the increase of the residual
603 circulation. An accelerated residual circulation increases the stratosphere-troposphere
604 mass exchange rate, which weakens the recirculation of tracers within the stratosphere.
605 In summary, both processes are related to the strengthening of the residual circulation,
606 but they impact different aspects of the age spectra.
607
608 The long-term changes in stratospheric mixing are investigated using the equivalent
609 length of N_2O. In the simulation, the tropical pipe becomes more leaky in its base at the
610 end of the 21st century. If there were no changes in tropical upwelling, the enhanced

611 mixing would increase the recirculation between the tropics and midlatitudes, which
612 would lead to older mean age, larger width, and longer tail. However, the increase of
613 isentropic mixing in the subtropical lower stratosphere is closely associated with the
614 increase of tropical upwelling. Our model results indicate that the impacts of increased
615 mixing on the age spectra are dominated by the acceleration of the residual circulation.
616
617 The mean age and chemical tracers respond differently to changes in the age spectra
618 because they are sensitive to different parts of the age spectra. The mean age weights
619 heavily on the tail of the age spectra, whereas the chemical tracers are more sensitive to
620 the head of the age spectra. Because young and old air masses change differently, the
621 mean age and chemical tracers have different long-term changes in the 21st century.
622 Clearly the age spectrum is more useful than the mean age to study chemical tracers.
623
624 **Acknowledgements.**
625
626 This work is supported by NASA's Modeling, Analysis and Prediction program. We
627 thank Stacey Frith for data management. Computational resources for this work were
628 provided by NASA's High-Performance Computing through the generous award of
629 computing time at NASA Ames Research Center.
630

References

Andrews, D. G., J. R. Holton, and C. B. Leovy (1987), Middle Atmosphere Dynamics, 485 pp., Academic, Orlando, Fla.

Austin, J., and F. Li (2006), On the relationship between the strength of the Brewer-Dobson circulation and the age of stratospheric air, *Geophys. Res. Lett., 33*, L17807, doi:10.1029/2006GL026867.

Boering, K. A., S. C. Wofsy, B. C. Daube, H. R. Schneider, M. Loewenstein, J. R. Podolske, T. J. Conway (1996), Stratospheric mean ages and transport rates from observations of carbon dioxide and nitrous oxide, *Science, 274*, 1340–1343.

Butchart, N., and A. A. Scaife (2001), Removal of chlorofluorocarbons by increased mass exchange between the stratosphere and troposphere in a changing climate. *Nature, 410,* 799–802.

Butchart, N., and Coauthors (2006), Simulations of anthropogenic change in the strength of the Brewer–Dobson circulation. *Clim. Dyn., 27*, 727–741.

Butchart, N., et al. (2010), Chemistry-climate model simulations of twenty-first century stratospheric climate and circulation change, *J. Clim., 23,* 5349-5374.

Douglass, A., R. Rood, S. Kawa, and D. Allen (1997), A three-dimensional simulation of the evolution of the middle latitude winter ozone in the middle stratosphere, *J. Geophys. Res., 102*(D15), 19217-19232.

Douglass, A. R., R. S. Stolarski, M. R. Schoeberl, C. H. Jackman, M. L. Gupta, P. A. Newman, J. E. Nielsen, and E. L. Fleming (2008), Relationship of loss, mean age of air and the distribution of CFCs to stratospheric circulation and implications for atmospheric lifetimes, *J. Geophys. Res.*, 113, D14309, doi:10.1029/2007JD009575.

Engel, A., Mobius, T., Bonisch, H., Schmidt, U., Heinz, R., Levin, I., Atlas, E., Aoki, S., Nakazawa, T., Sugawara, S., Moore, F., Hurst, D., Elkins, J., Schauffler, S., Andrews, A., and Boering, K. (2009), Age of stratospheric air unchanged within uncertainties over the pat 30 years, *Nature Geosci.*, *2*, 28–31.

Garcia, R. R., D. R. Marsh, D. E. Kinnison, B. A. Boville, and F. Sassi (2007), Simulation of secular trends in the middle atmosphere, 1950–2003, *J. Geophys. Res., 112*, D09301, doi:10.1029/2006JD007485.

Garcia, R. R., and W. Randel (2008), Acceleration of the Brewer–Dobson circulation due to increases in greenhouse gases. *J. Atmos. Sci.*, *65*, 2731–2739.

Garcia, R. R., W. J. Randel, D. E. Kinnison (2011), On the Determination of Age of Air Trends from Atmospheric Trace Species. *J. Atmos. Sci.*, *68*, 139–154. doi:10.1175/2010JAS3527.1

Haine, T. W. N., H. Zhang, D. W. Waugh, and M. Holzer (2008), On transit-time distributions in unsteady circulation models, *Ocean Modelling*, 21, 35-45.

Hall, T. M., and R. A. Plumb (1994), Age as a diagnostic of stratospheric transport, *J. Geophys. Res., 99*, 1059-1070.

Hall, T. H., D. J. Wuebbles, K. A. Boering, R. S. Eckman, J. Lerner, R. A. Plumb, D. H. Rind, C. P. Rinsland, D. W. Waugh, and C.-F. Wei (1999a), Transport experiments, in Models and Measurements Intercomparison II, edited by J. H. Park et al., Rep. NASA/TM-1999-20,9554, chap. 2, pp. 110–189, NASA, Hampton, Va.

Hall, T. M., D. W. Waugh, K. A. Boering, and R. A. Plumb (1999b), Evaluation of transport in stratospheric models, *J. Geophys. Res., 104*, 18815-18839.

Holzer, M., I. G. McKendry, and D. A. Jaffe (2003), Springtime trans-Pacific atmospheric transport from east Asia: A transit-time probability density function approach, *J. Geophys. Res.*, 108(D22), 4708, doi:10.1029/2003JD003558.

Holton, J. R., P. H. Haynes, M. E. McIntyre, A. R. Douglass, R. B. Rood, and L. Pfister (1995), Stratosphere-troposphere exchange, *Rev. Geophys.*, *33*(4), 403–439, doi:10.1029/95RG02097.

Intergovernmental Panel on Climate Change (2001), Climate Change 2001: The scientific basis. Contribution of Working Group 1 to the Third Assessment Report, edited by J. T. Houghton et al., Cambridge Univ. Press, New York.

Li, F., J. Austin, and J. Wilson (2008), The strength of the Brewer–Dobson circulation in a changing climate: Coupled chemistry–climate model simulations. *J. Climate*, *21*, 40-57.

Li., F., D. Waugh, A. R. Douglass, P. A. Newman, S. Pawson, R. S. Stolarski, S. E. Strahan, and J. E. Nielsen (2012), Seasonal variations of stratospheric age spectra in GEOSCCM, *J. Geophys. Res.*, doi:10.1029/2011JD016877, in press.

Ma, J., D. W. Waugh, A. R. Douglass, S. R. Kawa, and S.-J. Lin (2003), Evaluation of the transport in the Goddard Space Flight Center three-dimensional chemical transport model using the equivalent length diagnostic, *J. Geophys. Res., 108*(D6), 4201, doi:10.1029/2002JD002268.

McLandress, C., and T. G. Shepherd (2009), Simulated anthropogenic changes in the Brewer-Dobson circulation, including its extension to high latitudes, *J. Clim*ate, ***22,*** 1516–1540.

Nakamura, N. (1996), Two-dimensional mixing, edge formation, and permeability diagnosed in an area coordinate, *J. Atmos. Sci.*, 53, 1524–1537.

Neu, J. L., and R. A. Plumb (1999), Age of air in a ''leaky pipe'' model of stratospheric transport, *J. Geophys. Res., 104,* 19,243– 19,255.

Oman, L., D. W. Waugh, S. Pawson, R. S. Stolarski, and P. A. Newman (2009), On the influence of anthropogenic forcings on changes in the stratospheric mean age, *J. Geophys. Res., 114*, D03105, doi:10.1029/2008JD010378.

Pawson, S., R. S. Stolarski, A. R. Douglass, P. A. Newman, J. E. Nielsen, S. M. Frith, and M. L. Gupta (2008), Goddard Earth Observing System chemistry climate model simulations of stratosphere ozone temperature coupling between 1950 and 2005, *J. Geophys. Res., 113*(D12), D12103, doi:10.1029/2007JD009511.

Prather, M. J. (1996), Time scales in atmospheric chemistry: Theory, GWPs for CH4 and CO, and runaway growth, *Geophys. Res. Lett., 23*, 2597-2600.

Ray, E. A., et al. (2010), Evidence for changes in stratospheric transport and mixing over the past three decades based on multiple data sets and tropical leaky pipe analysis, *J. Geophys. Res., 115*, D21304, doi:10.1029/2010JD014206.

Rienecker, M. M., et al. (2008), The GEOS-5 data assimilation system—Documentation of versions 5.0.1, 5.1.0, and 5.2.0, NASA Tech. Memo., NASA TM-2008-104606, vol. 27, 118 pp.

Schauffler, S. M., E. L. Atlas, S. G. Donnelly, A. Andrews, S. A. Montzka, J. W. Elkins, D. F. Hurst, P. A. Romashkin, G. S. Dutton, and V. Stroud (2003), Chlorine budget and partitioning during the Stratospheric Aerosol and Gas Experiment (SAGE) III Ozone Loss and Validation Experiment (SOLVE), J. *Geophys. Res., 108*(D5), 4173, doi:10.1029/2001JD002040.

Schoeberl, M. R., A. R. Douglass, Z. Zhu, and S. Pawson (2003), A comparison of the lower stratospheric age spectra derived from a general circulation model and two data assimilation systems, *J. Geophys. Res., 108*(D3), 4113, doi:10.1029/2002JD002652.

Schoeberl, M. R., A. R. Douglass, B. Polansky, C. Boone, K. A. Walker, and P. Bernath (2005), Estimation of stratospheric age spectrum from chemical tracers, *J. Geophys. Res., 110*, D21303, doi:10.1029/2005JD006125.

Schoeberl, M. R., A. R. Douglass, R. S. Stolarski, S. Pawson, S. E. Strahan, and W. Read (2008), Comparison of lower stratospheric tropical mean vertical velocities, *J. Geophys. Res., 113*, D24109, doi:10.1029/2008JD010221.

Shepherd, T. G. (2002), Issues in stratosphere-troposphere coupling, *J. Meteo. Soc. Japan, 80*, 769-792.

Shepherd, T. G., and C. McLandress (2011), A robust mechanism for strengthening of the Brewer–Dobson circulation in response to climate change: Critical-layer control of subtropical wave breaking, *J. Atmos. Sci.*, *68*, 784–797. doi: 10.1175/2010JAS3608.1

SPARC CCMVal (2010), SPARC CCMVal Report on the Evaluation of Chemistry-Climate Models, V. Eyring, T. G. Shepherd, D. W. Waugh (Eds.), SPARC Report No. 5, WCRP-X, WMO/TD-No. X, http://www.atmosp.physics.utoronto.ca/SPARC.

Strahan, S. E., M. R. Schoeberl, and S. D. Steenrod (2009), The impact of tropical recirculation of polar composition, *Atmos. Chem. Phys., 9*, 2471-2480.

Strahan, S. E., et al. (2011), Using transport diagnostics to understand chemistry climate model ozone simulations, *J. Geophys. Res.*, *116*, D17302, doi:10.1029/2010JD015360.

Waugh, D. W., and T. M. Hall (2002), Age of stratospheric air: Theory, observations, and models, *Rev. Geophys., 40*(4), 1010.doi:10.1029/2009RG000101.

Waugh, D. W., S. E. Strahan, and P. A. Newman (2007), Sensitivity of stratospheric inorganic chlorine to differences in transport, *Atmos. Chem. Phys, 7*, 4935-4941.

Figure Captions:

Figure 1: Examples of the Boundary Impulse Responses (BIRs) in 2000-2019 at three locations. For this 20-year period, five BIRs are released in January (red) and five BIRs are released in July (blue) of 2000-2004. The thick black line is the age spectrum, which is calculated as the mean of the ten BIRs. The unit is 1/month.

Figure 2: (a) Distribution of the 2000 age spectrum mean age (lines) and the differences in the mean age between the 2080 and 2000 age spectra (color). (b) Distribution of the residual vertical velocity for the period 2000-2019 (lines) and the differences in the residual vertical velocity between 2080-2099 and 2000-2019 (color). (c) Same as Figure 2b, but for the residual meridional velocity.

Figure 3: (a) Comparison of the mean age (dashed), modal age (dotted), and the timescale of the residual vertical velocity in the tropical pipe region (10°S – 10°N, 70hPa – 1 hPa) in the period 2000-2019. The error bars represent interannual variations of these three timescales. (b) Difference in the mean age (dashed), model age (dotted) and the timescale of the residual velocity in the tropical pipe region between 2080-2099 and 2000-2019.

Figure 4: The color shadings are differences in the modal age (left) and spectral width (right) between the 2080 and 2000 age spectra. The contours are the modal age (left) and spectra width (right) of the 2000 age spectra.

Figure 5: (a) Distribution of the 2000 age spectra at 50 hPa as a function of latitude. The black solid, dashed, and dotted lines are the mean age, spectral width, and modal age, respectively. (b) Differences between the 2080 and 2000 age spectra at 50 hPa. The black lines are the same as in panel (a). The green solid, dashed, and dotted lines are the mean age, spectral width, and modal age in the 2080 age spectra, respectively. In both panels the color scales are normalized to the maximum value shown at the top of the color bar. The unit is 1/month.

Figure 6: Same as Figure 5, but for age spectra at 10 hPa.

Figure 7: Evolution of the age spectra in the 21st century at different locations at 50 hPa.

Figure 8: Same as Figure 7, but on logarithmic scale.

Figure 9: (a) The scatter plot of the decay timescale of the tail of the age spectra against the globally and stratospheric averaged (100 – 1 hPa) mean age. (b) The scatter plot of the tail decay timescale against the tropical upward mass flux at 70 hPa. The error bars represent the interannual variations of these diagnostics.

Figure 10: (a) The fractional contribution of tail to the mean age in the 2000 age spectra (lines) and the differences between the 2080 and 2000 age spectra (colors). The tail is defined as the region with transit time older than 4 years. (b) Same as Figure 10a, but for the averaged transit time in the tail region.

Figure 11: Distribution of the normalized equivalent length squared of N_2O for the period 2000-2019 (lines) and the percentage changes between 2080-2099 and 2000-2019 (colors). Only differences statistically significant at the 95% confidence level are shown.

Figure 12: (a) Color shadings are differences in temperature between 2080-2099 and 2000-2019. Lines are 2000-2019 mean. (b) Same as Figure 12a, but for the zonal wind.

Figure 13: (a) The scatter plot of the equivalent length squared of N_2O in the subtropical lower stratosphere (averaged in10°-30° latitudes and 440-520 K) against topical upward mass flux at 70 hPa (black, left axis), and the scatter plot of the equivalent length squared of N_2O against the zonal wind in the subtropical UTLS (averaged in 10°-30° latitudes and 200-70 hPa, blue, right axis). (b) The scatter plot of the equivalent length squared of N_2O in the subtropical lower stratosphere against the mean age (black) and spectral width (blue) in the subtropical lower stratosphere (averaged in 10°-30° latitudes and 70-50 hPa).

Figure 14: (a) Comparison of the compact relationship between the mean age and N_2O in the northern hemisphere 100-50 hPa between 2000-2019 (black) and 2080-2099 (red). (b) Same as Figure 14a, but for the relationship between the mean age and the fractional release of CFC12.

Figure 15: Evolution of the stratospheric mass burden of three radioactive tracers with different decay rate (black solid), the mean age tracer (black dashed), CFC11 (green) and CFC12 (blue) in the 21st century relative to their respective 2000-2019 level.

Figure 16: (a) Changes of stratospheric air masses between the 2080 and 2000 age spectra relative to the total stratospheric mass burden as a function of transit time at 1-year interval. (b) Changes of stratospheric air masses between the 2080 and 2000 age spectra relative to their 2000 level.

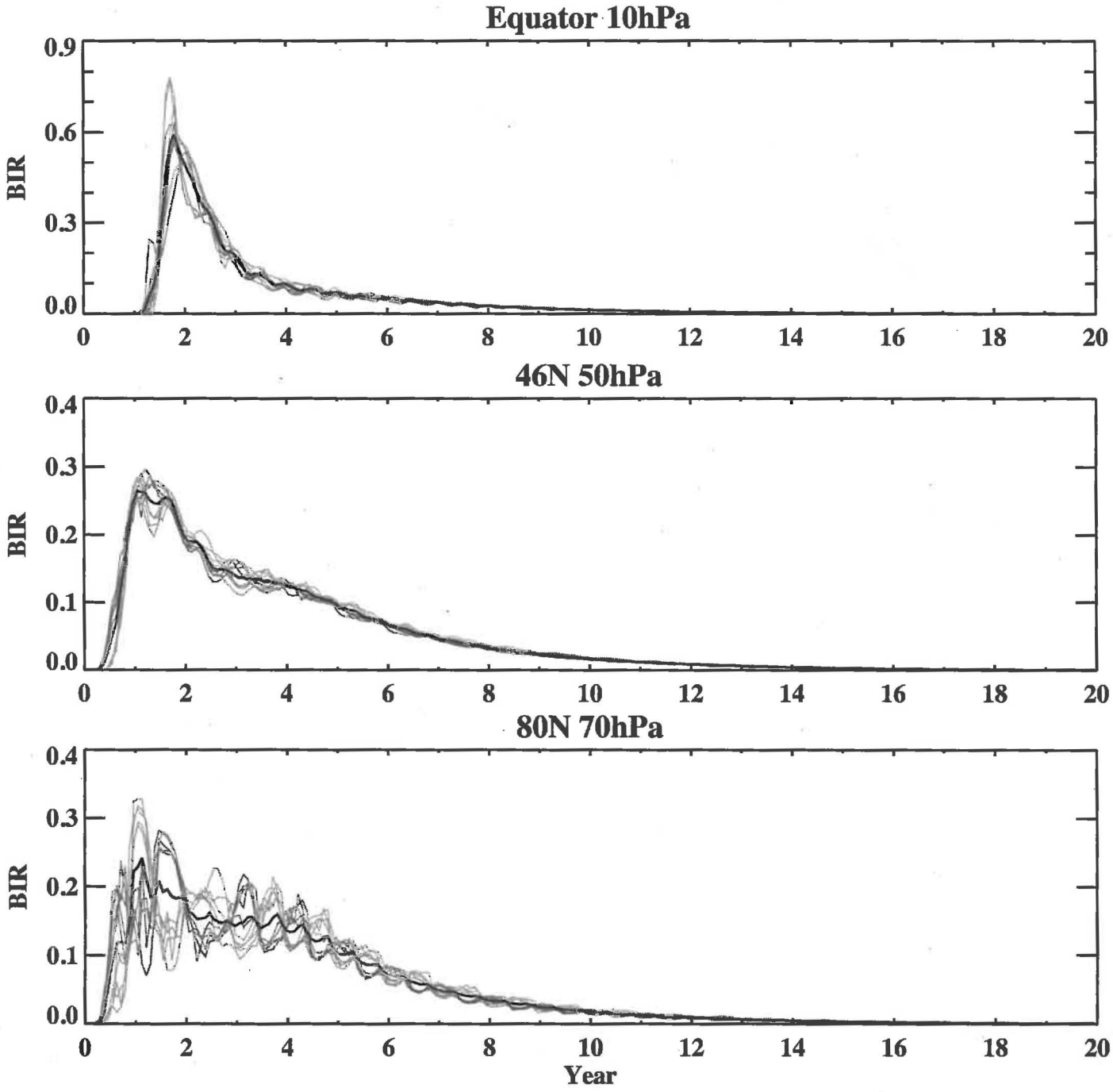
Equator 10hPa
BIR
0.9
0.6
0.3
0.0
0 2 4 6 8 10 12 14 16 18 20
46N 50hPa
BIR
0.4
0.3
0.2
0.1
0.0
0 2 4 6 8 10 12 14 16 18 20
80N 70hPa
BIR
0.4
0.3
0.2
0.1
0.0
0 2 4 6 8 10 12 14 16 18 20
Year

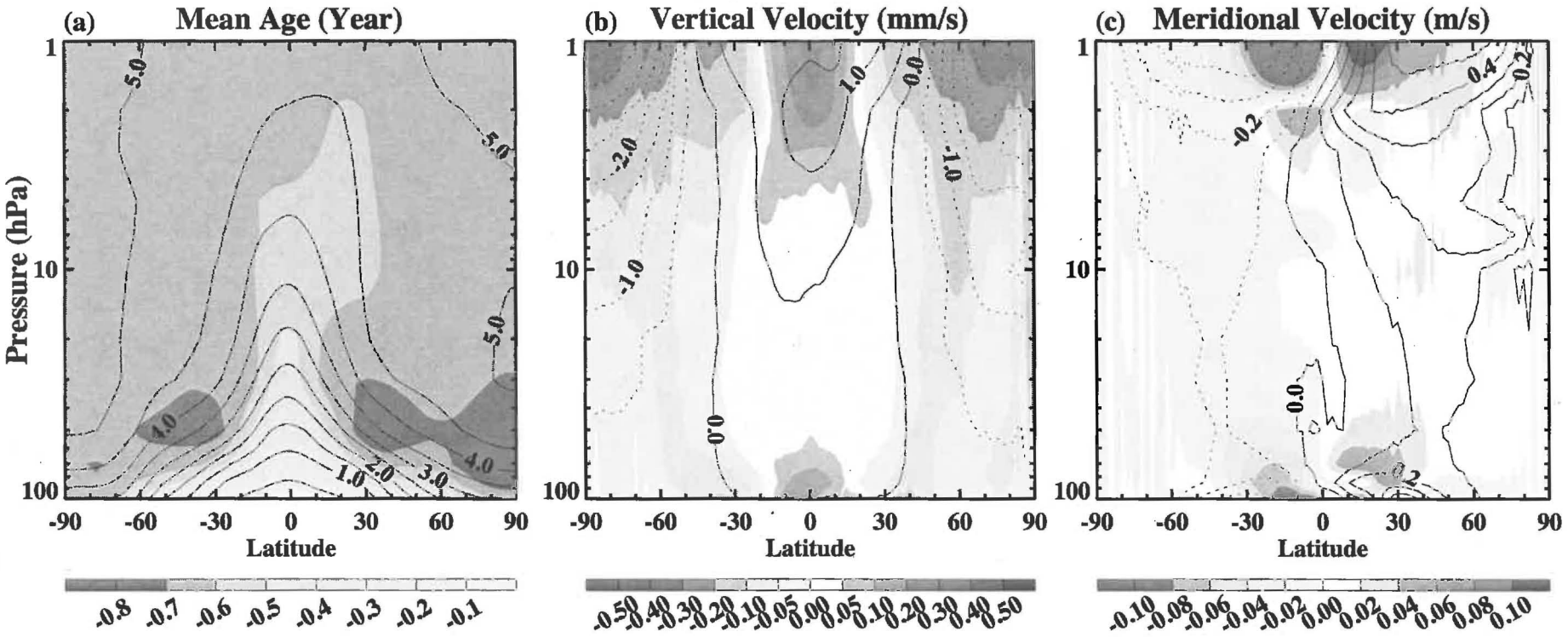
(a) Mean Age (Year)
(b) Vertical Velocity (mm/s)
(c) Meridional Velocity (m/s)
Pressure (hPa)
1
10
100
-90 -60 -30 0 30 60 90
Latitude
5.0
4.0
3.0
2.0
1.0
-2.0
-1.0
0.0
1.0
0.4
0.2
-0.2
0.0
.8 .7 .6 .5 .4 .3 .2 .1
.50 .40 .30 .20 .10 .05 .00 .05 .10 .20 .30 .40 .50
.10 .08 .06 .04 .02 .00 .02 .04 .06 .08 .10

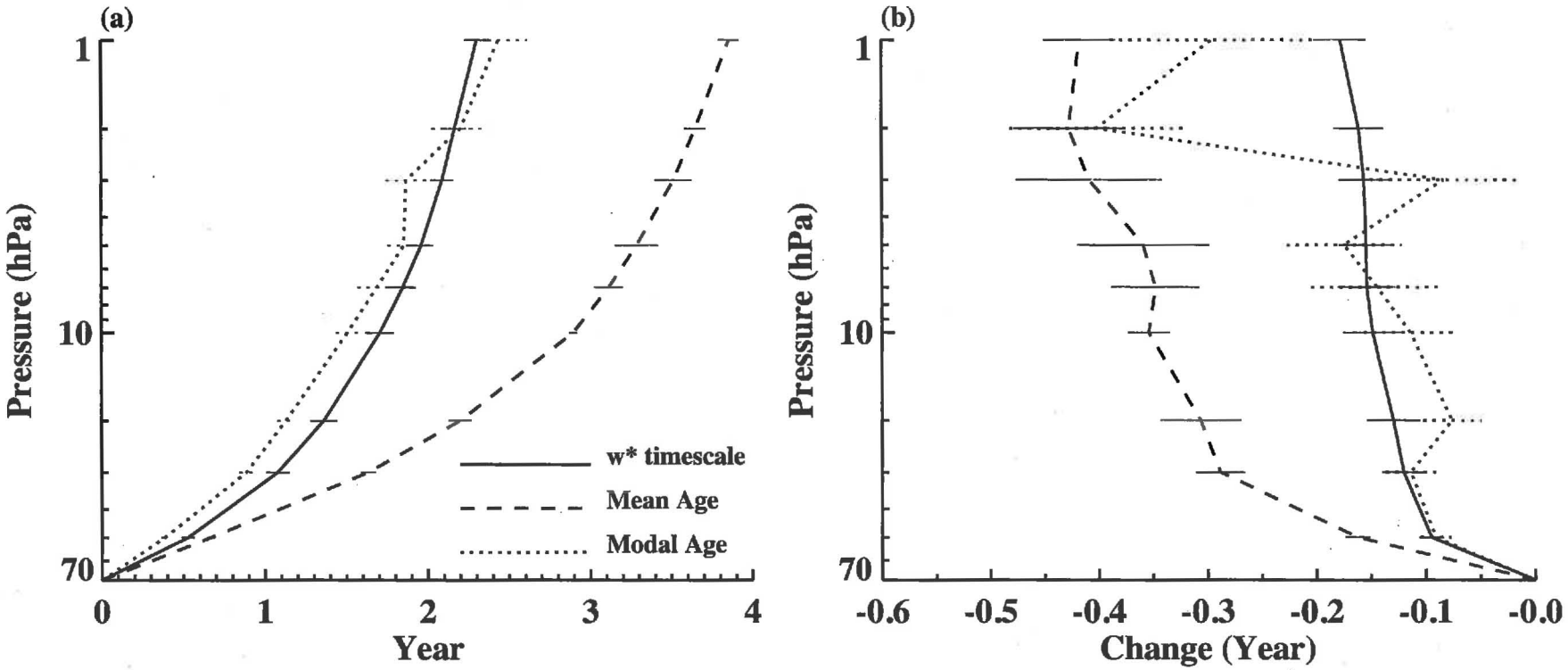
(a)
1
10
70
Pressure (hPa)
0
1
2
3
4
Year
w* timescale
Mean Age
Modal Age
(b)
1
10
70
Pressure (hPa)
-0.6
-0.5
-0.4
-0.3
-0.2
-0.1
-0.0
Change (Year)

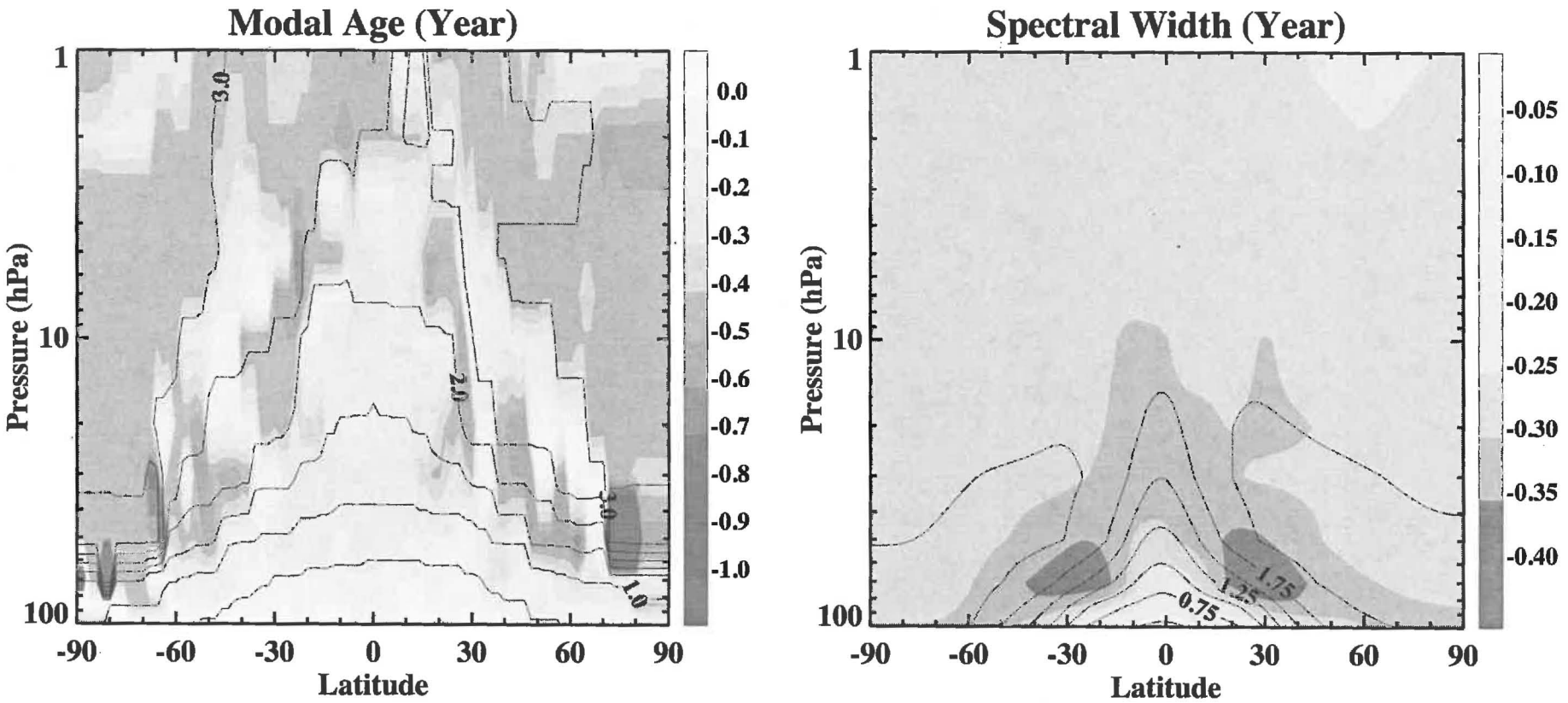
Modal Age (Year)
Pressure (hPa)
1
10
100
-90
-60
-30
0
30
60
90
Latitude
3.0
2.0
1.0
0.0
-0.1
-0.2
-0.3
-0.4
-0.5
-0.6
-0.7
-0.8
-0.9
-1.0
Spectral Width (Year)
Pressure (hPa)
1
10
100
-90
-60
-30
0
30
60
90
Latitude
1.75
1.25
0.75
-0.05
-0.10
-0.15
-0.20
-0.25
-0.30
-0.35
-0.40

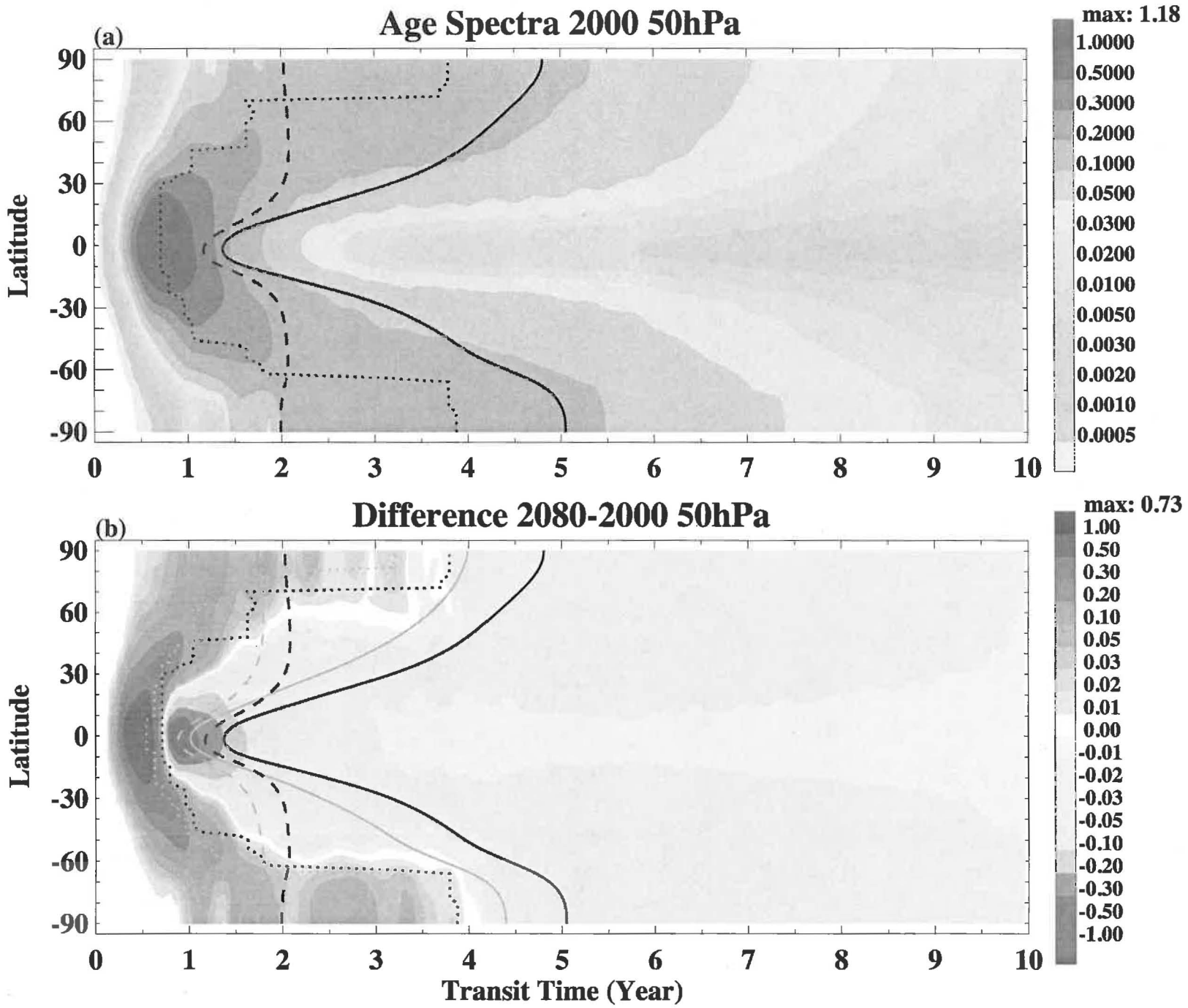
Age Spectra 2000 50hPa
(a)
max: 1.18
1.0000
0.5000
0.3000
0.2000
0.1000
0.0500
0.0300
0.0200
0.0100
0.0050
0.0030
0.0020
0.0010
0.0005
Latitude
90
60
30
0
-30
-60
-90
0
1
2
3
4
5
6
7
8
9
10
Difference 2080-2000 50hPa
(b)
max: 0.73
1.00
0.50
0.30
0.20
0.10
0.05
0.03
0.02
0.01
0.00
-0.01
-0.02
-0.03
-0.05
-0.10
-0.20
-0.30
-0.50
-1.00
Latitude
Transit Time (Year)

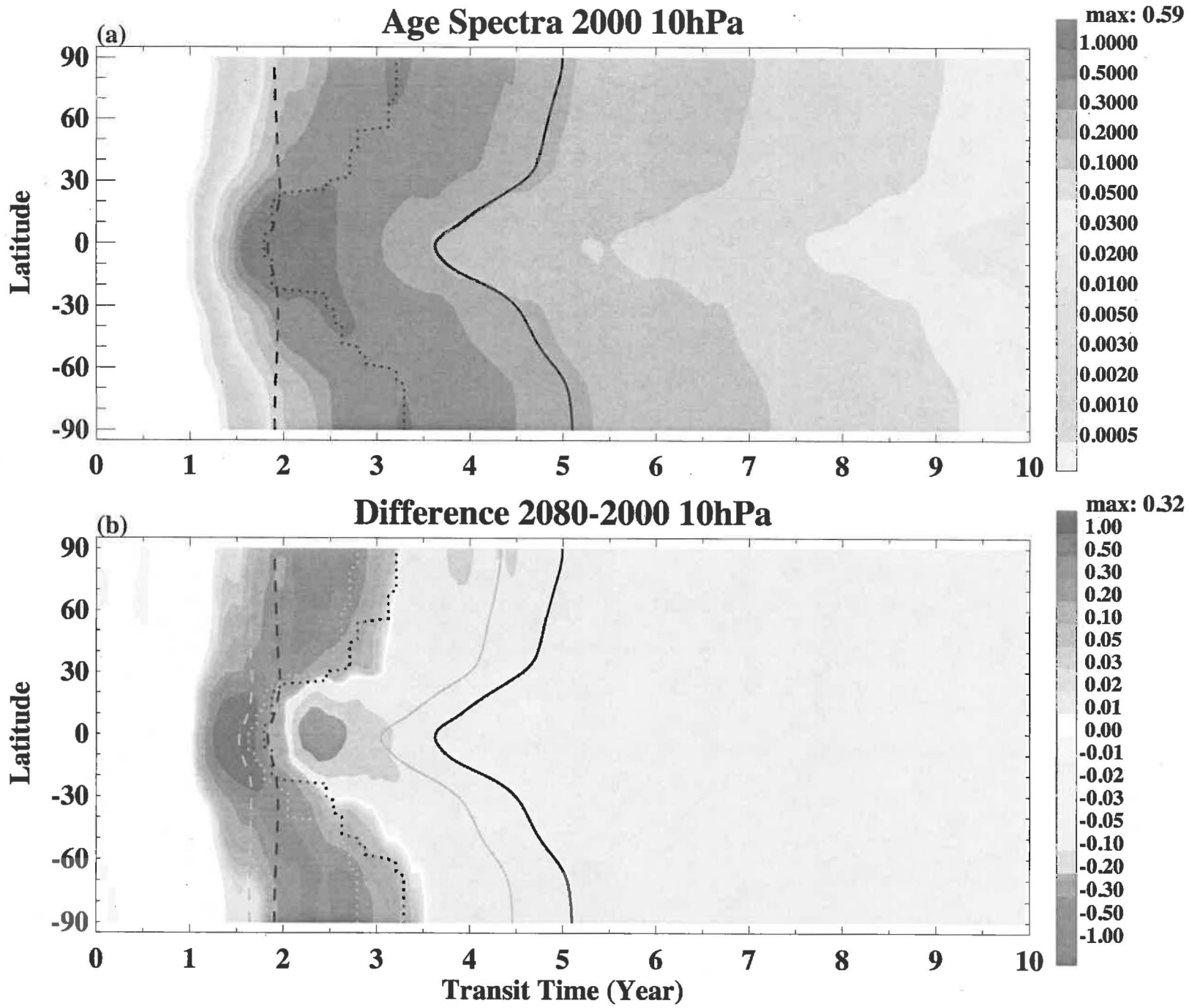
Age Spectra 2000 10hPa
(a)
max: 0.59
1.0000
0.5000
0.3000
0.2000
0.1000
0.0500
0.0300
0.0200
0.0100
0.0050
0.0030
0.0020
0.0010
0.0005
Latitude
90
60
30
0
-30
-60
-90
0
1
2
3
4
5
6
7
8
9
10
Difference 2080-2000 10hPa
(b)
max: 0.32
1.00
0.50
0.30
0.20
0.10
0.05
0.03
0.02
0.01
0.00
-0.01
-0.02
-0.03
-0.05
-0.10
-0.20
-0.30
-0.50
-1.00
Latitude
Transit Time (Year)

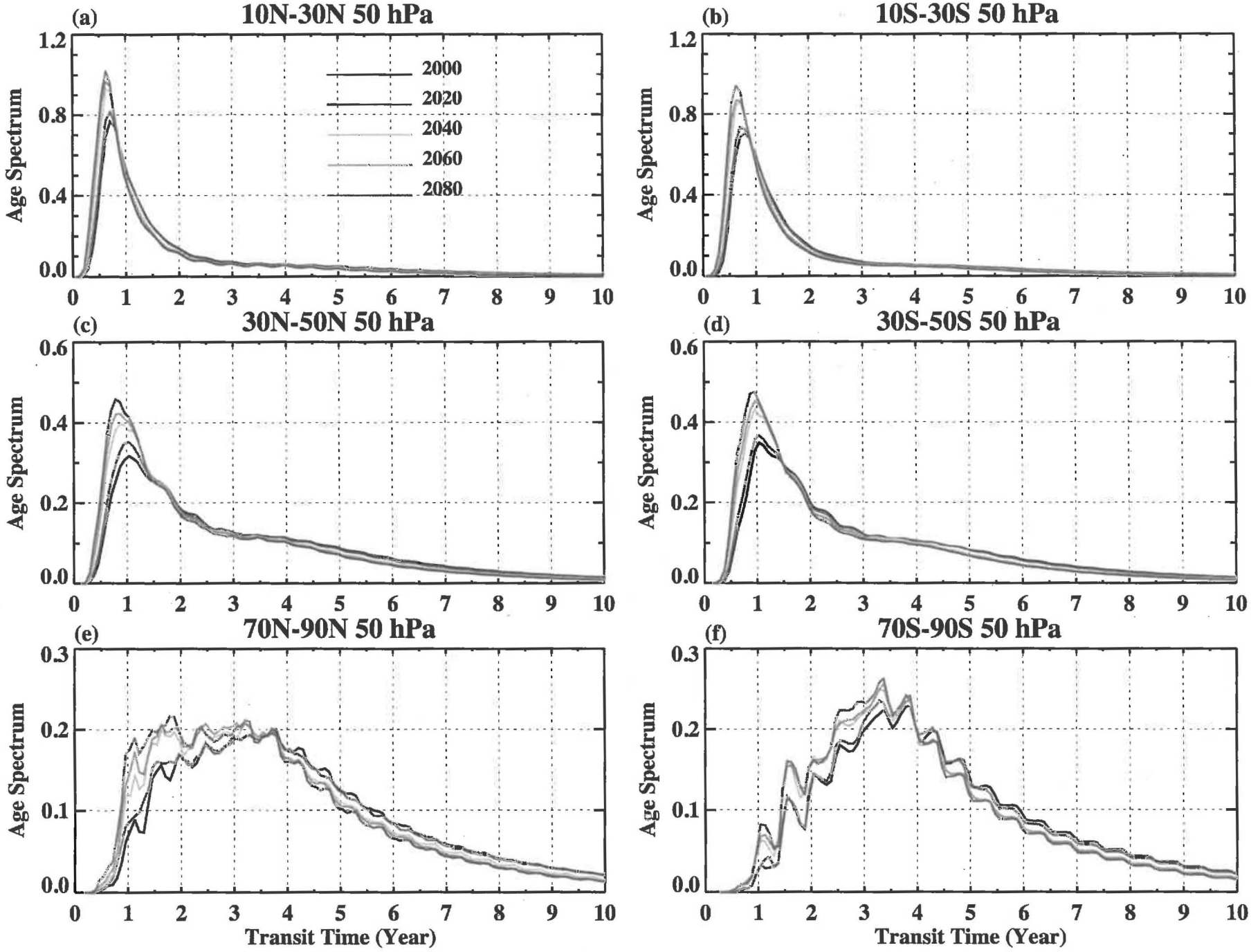
(a)
10N-30N 50 hPa
(b)
10S-30S 50 hPa
(c)
30N-50N 50 hPa
(d)
30S-50S 50 hPa
(e)
70N-90N 50 hPa
(f)
70S-90S 50 hPa
2000
2020
2040
2060
2080
Age Spectrum
Transit Time (Year)

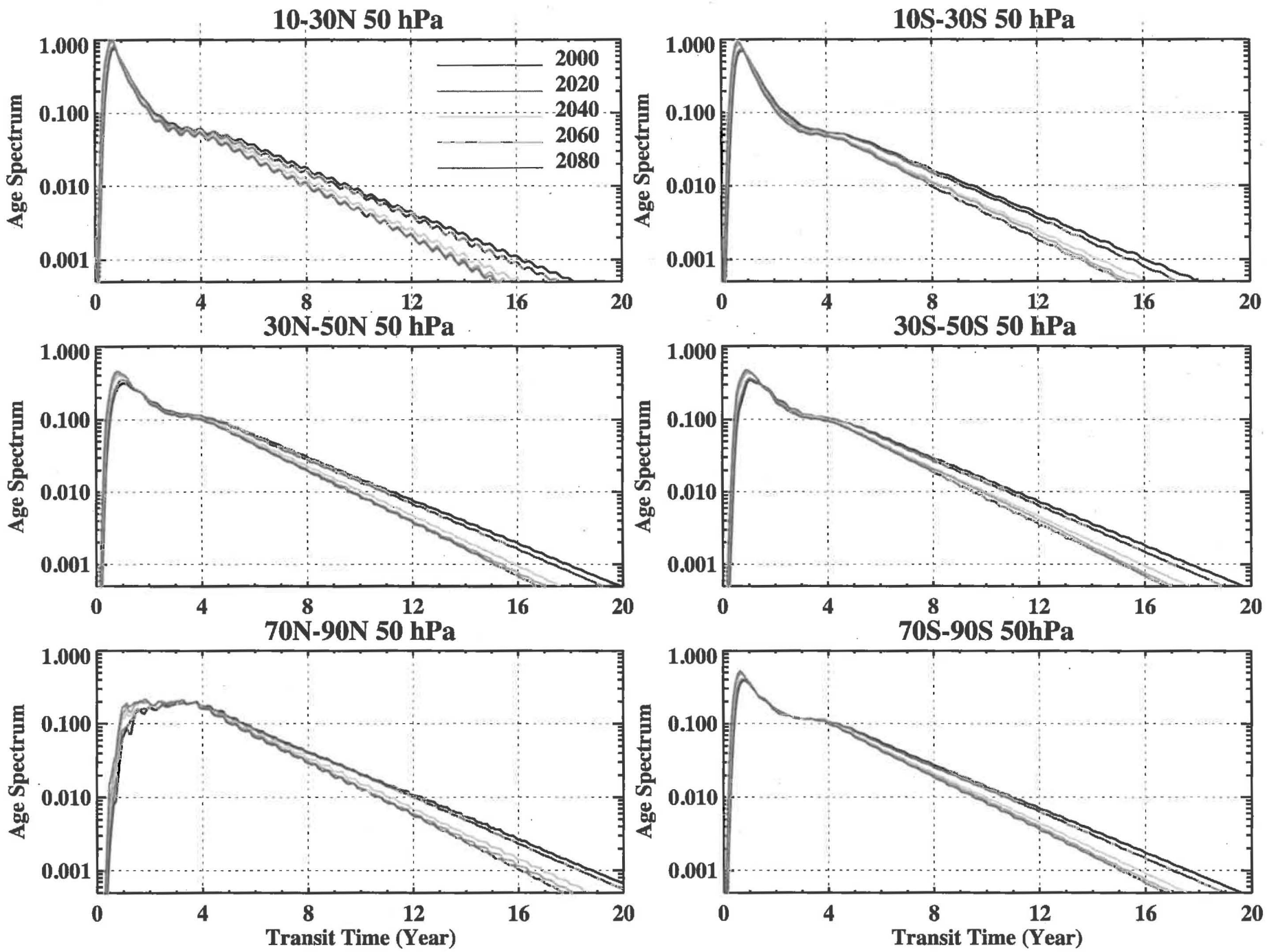
10-30N 50 hPa
10S-30S 50 hPa
30N-50N 50 hPa
30S-50S 50 hPa
70N-90N 50 hPa
70S-90S 50hPa
2000
2020
2040
2060
2080
Age Spectrum
1.000
0.100
0.010
0.001
0
4
8
12
16
20
Transit Time (Year)

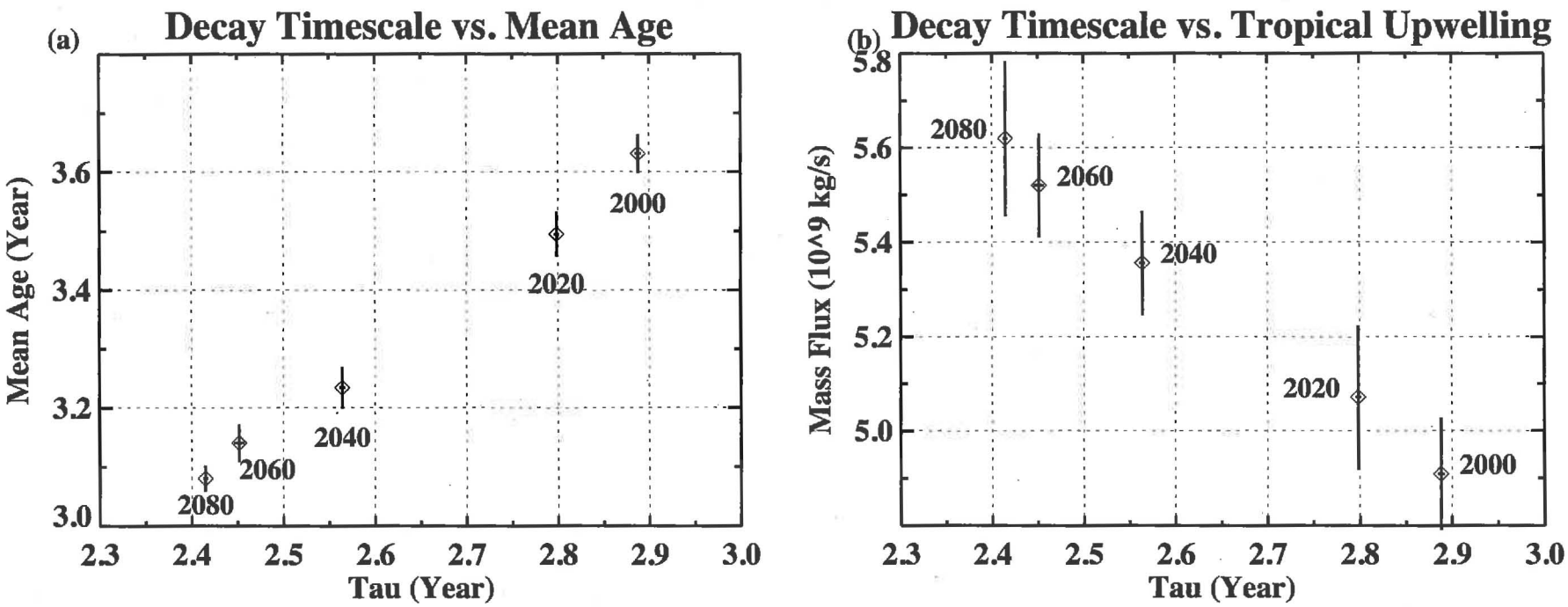
(a)
Decay Timescale vs. Mean Age
Mean Age (Year)
3.0
3.2
3.4
3.6
2080
2060
2040
2020
2000
2.3
2.4
2.5
2.6
2.7
2.8
2.9
3.0
Tau (Year)
(b)
Decay Timescale vs. Tropical Upwelling
Mass Flux (10^9 kg/s)
5.0
5.2
5.4
5.6
5.8
2080
2060
2040
2020
2000
2.3
2.4
2.5
2.6
2.7
2.8
2.9
3.0
Tau (Year)

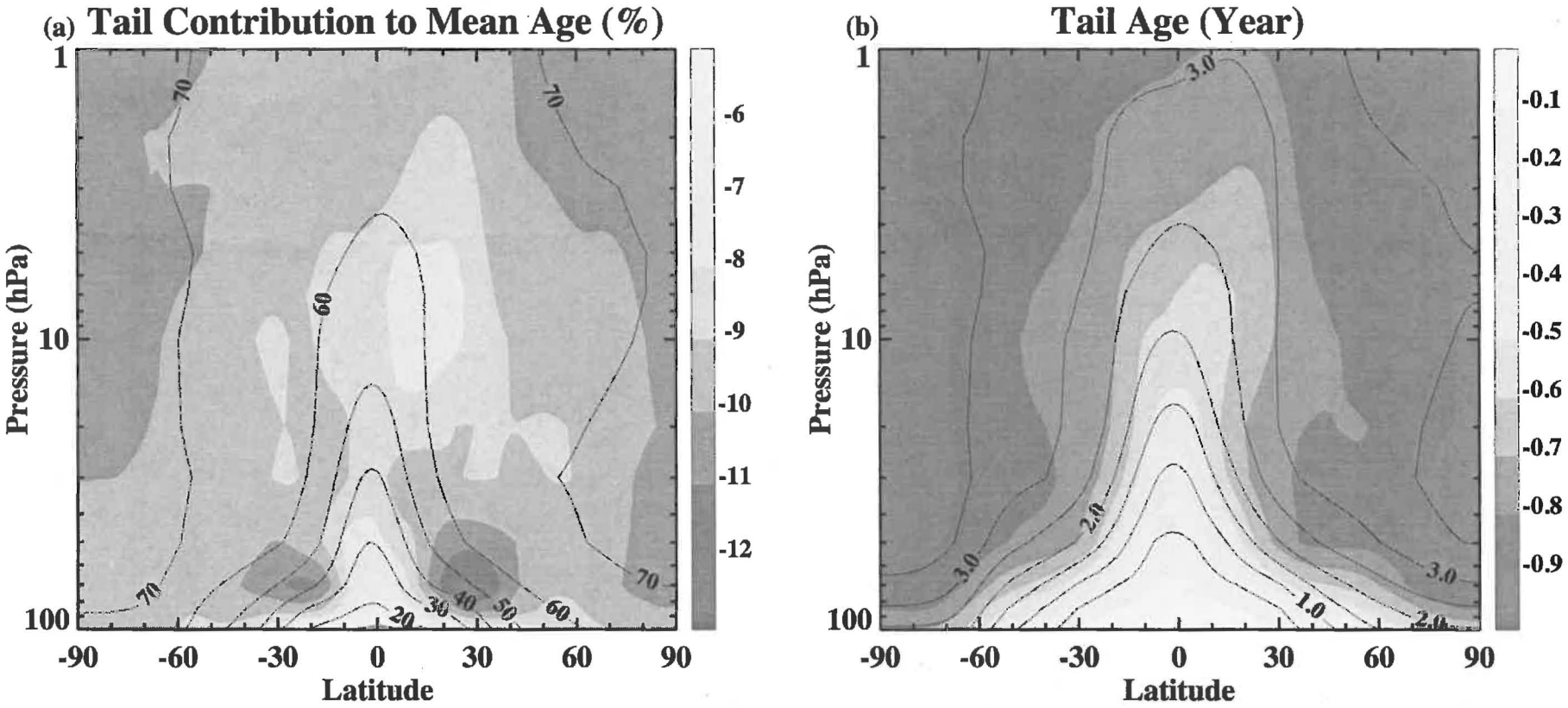
(a) Tail Contribution to Mean Age (%)
Pressure (hPa)
1
10
100
-90
-60
-30
0
30
60
90
Latitude
70
60
20
30
40
50
-6
-7
-8
-9
-10
-11
-12
(b)
Tail Age (Year)
3.0
2.0
1.0
-0.1
-0.2
-0.3
-0.4
-0.5
-0.6
-0.7
-0.8
-0.9

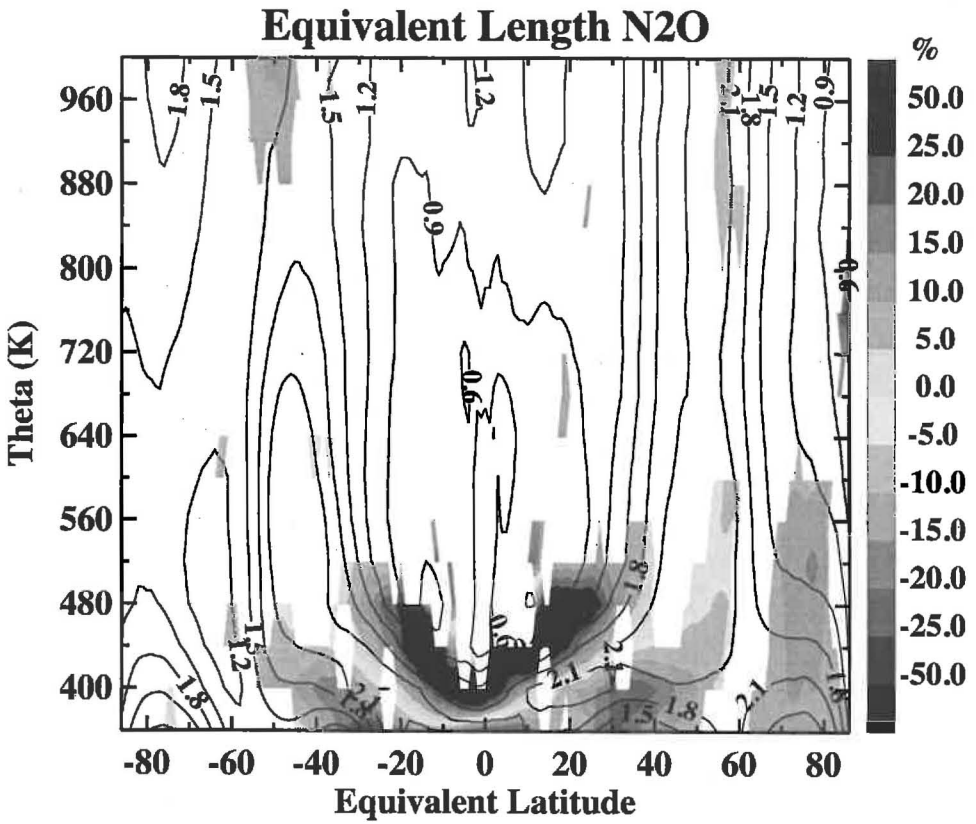
Equivalent Length N2O
Theta (K)
960
880
800
720
640
560
480
400
-80
-60
-40
-20
0
20
40
60
80
Equivalent Latitude
%
50.0
25.0
20.0
15.0
10.0
5.0
0.0
-5.0
-10.0
-15.0
-20.0
-25.0
-50.0

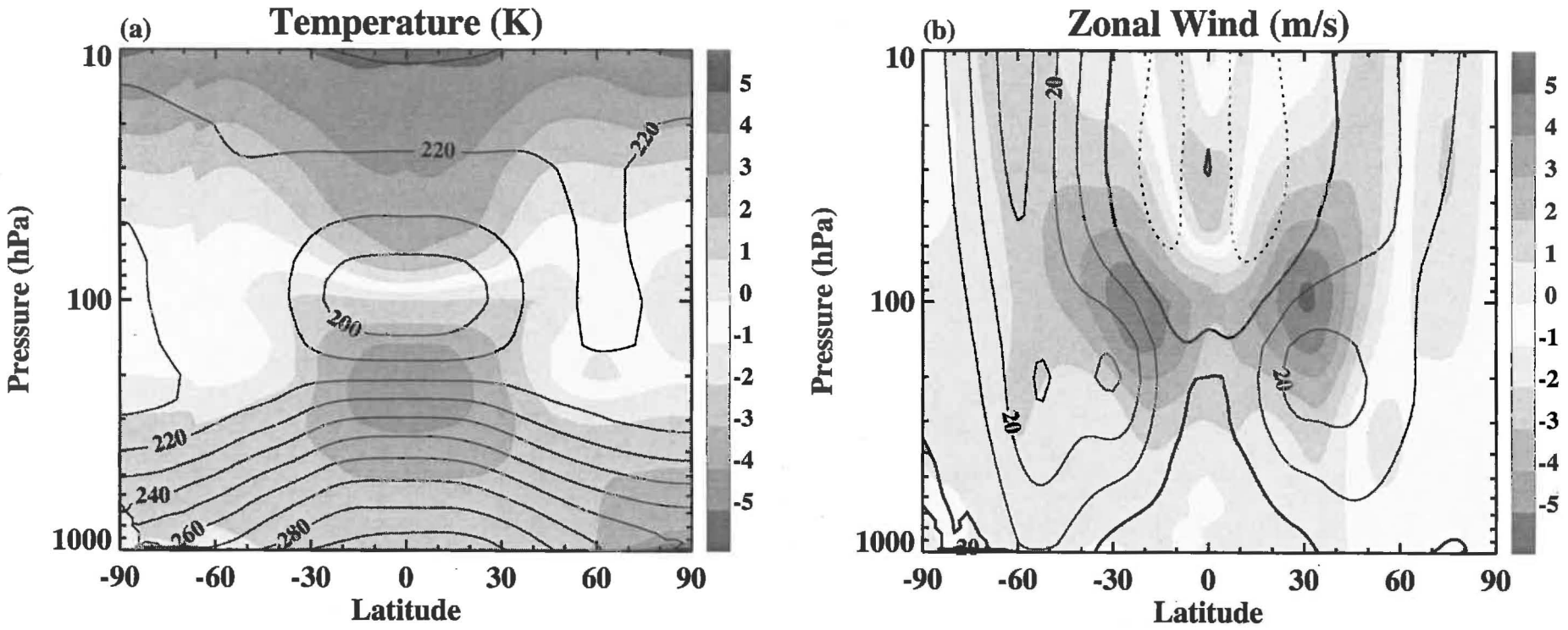
(a)
Temperature (K)
Pressure (hPa)
10
100
1000
-90
-60
-30
0
30
60
90
Latitude
220
200
240
260
280
5
4
3
2
1
0
-1
-2
-3
-4
-5
(b)
Zonal Wind (m/s)
Pressure (hPa)
10
100
1000
-90
-60
-30
0
30
60
90
Latitude
20
-20
5
4
3
2
1
0
-1
-2
-3
-4
-5

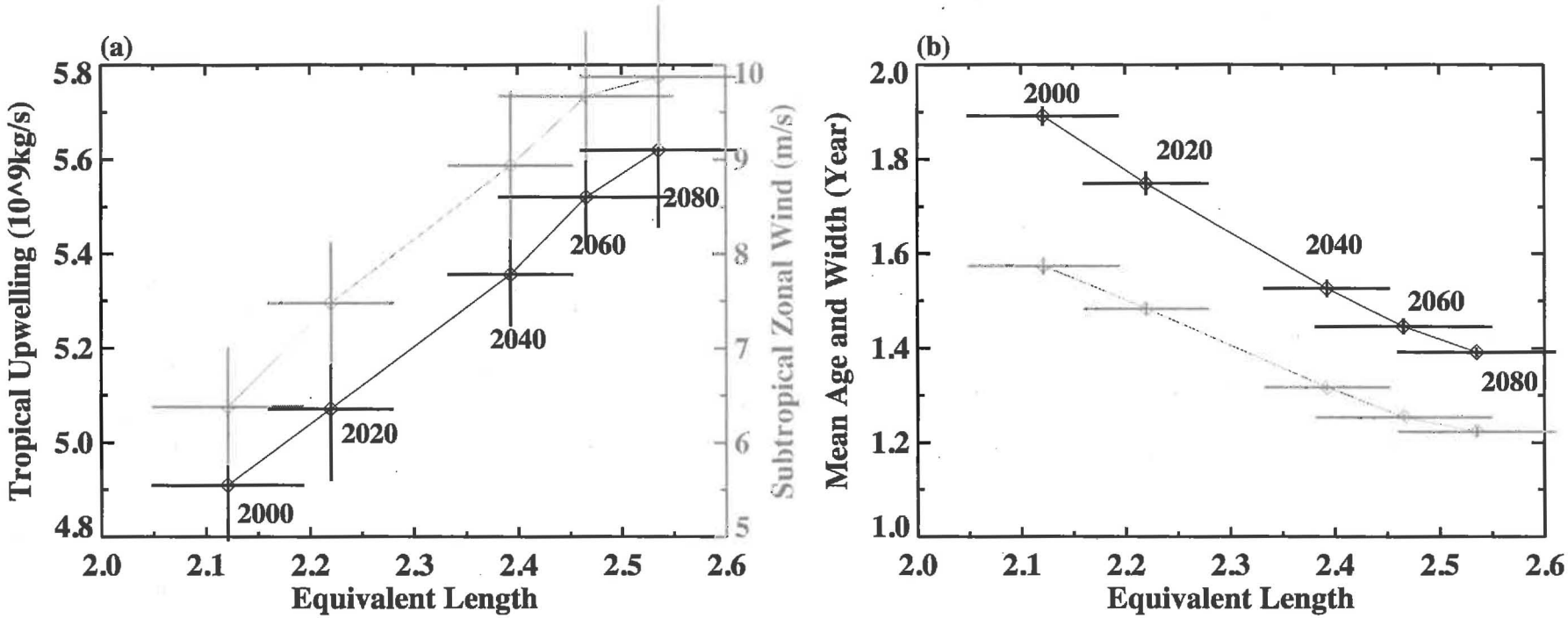
(a)
Tropical Upwelling (10^9kg/s)
Subtropical Zonal Wind (m/s)
Equivalent Length
2000
2020
2040
2060
2080
(b)
Mean Age and Width (Year)
Equivalent Length
2000
2020
2040
2060
2080

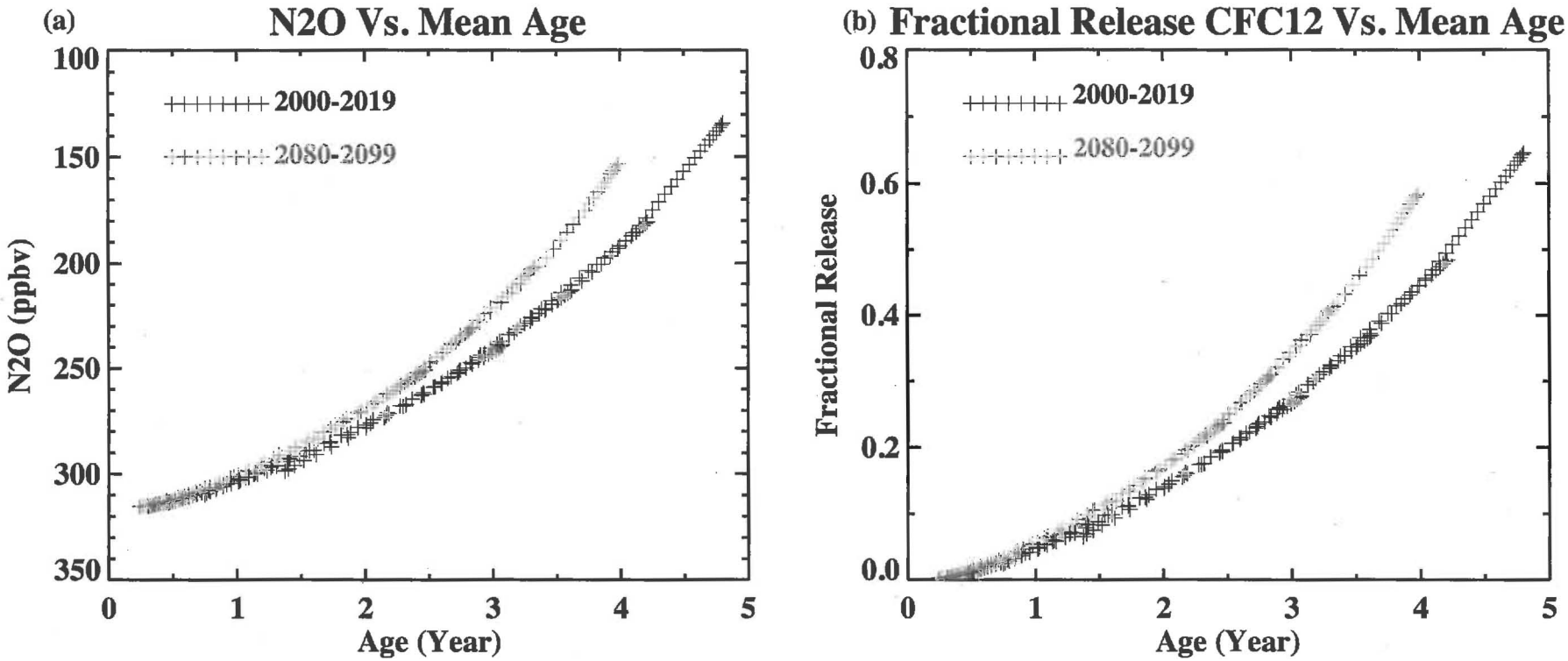
(a)
N2O Vs. Mean Age
2000-2019
2080-2099
N2O (ppbv)
100
150
200
250
300
350
0
1
2
3
4
5
Age (Year)
(b) Fractional Release CFC12 Vs. Mean Age
2000-2019
2080-2099
Fractional Release
0.0
0.2
0.4
0.6
0.8
0
1
2
3
4
5
Age (Year)

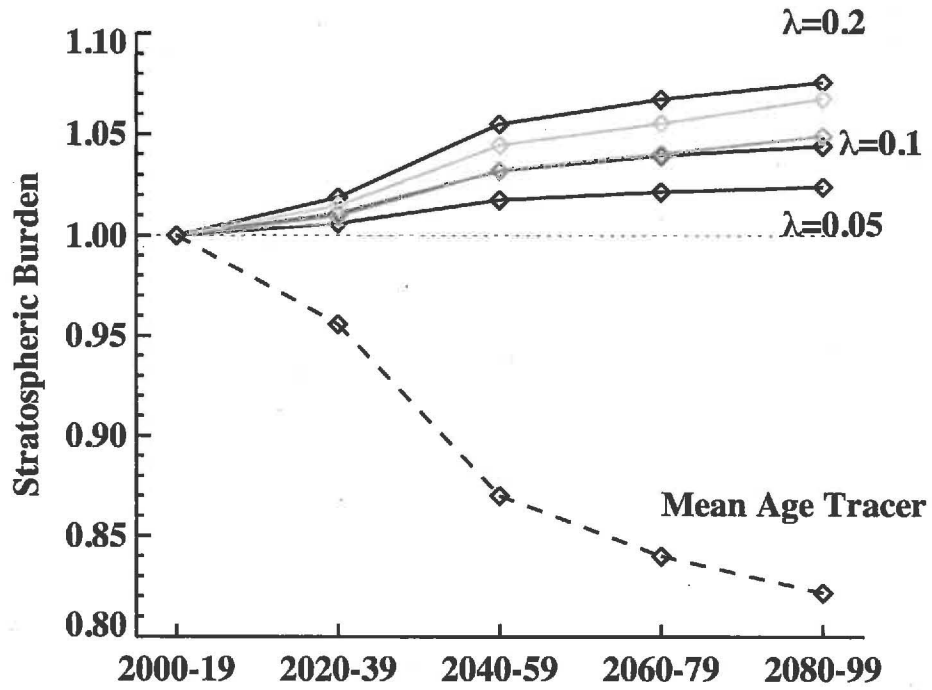
λ=0.2
λ=0.1
λ=0.05
Mean Age Tracer
Stratospheric Burden
1.10
1.05
1.00
0.95
0.90
0.85
0.80
2000-19
2020-39
2040-59
2060-79
2080-99

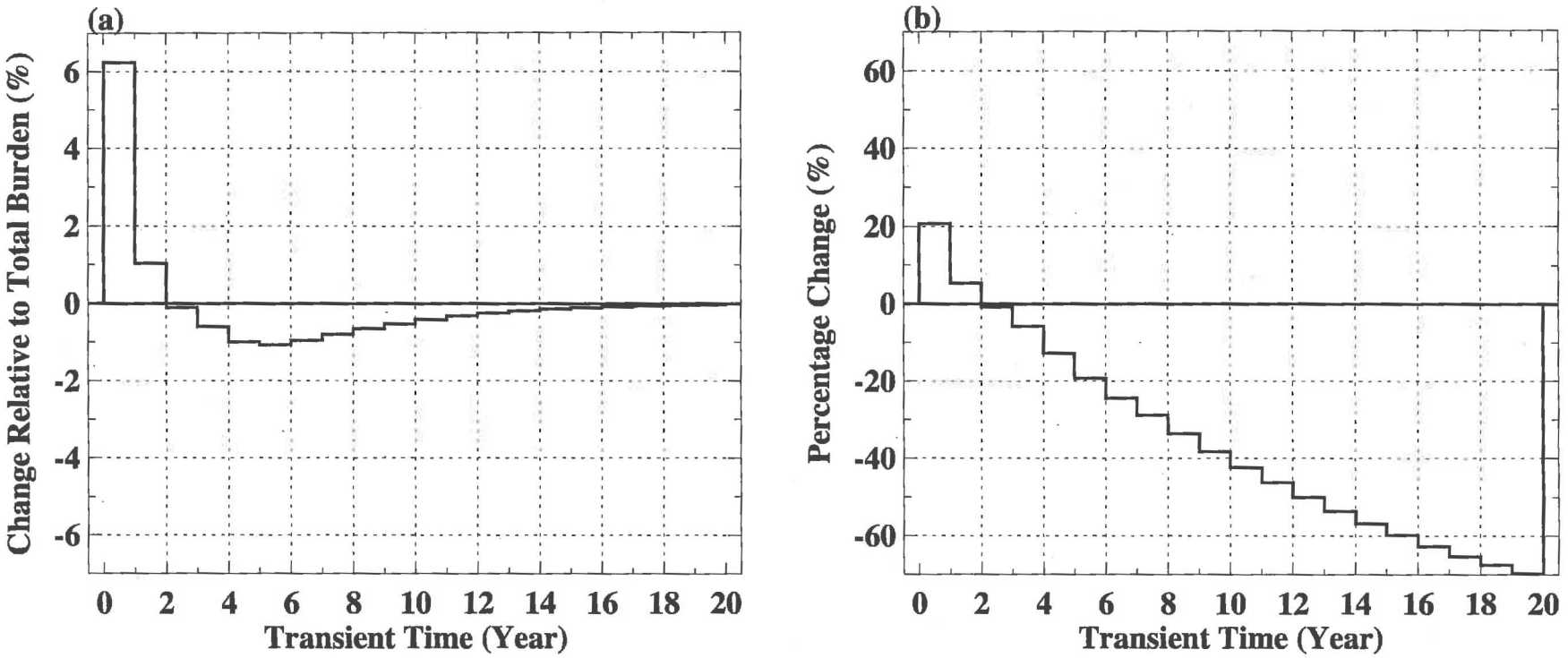
(a)
Change Relative to Total Burden (%)
6
4
2
0
-2
-4
-6
0 2 4 6 8 10 12 14 16 18 20
Transient Time (Year)
(b)
Percentage Change (%)
60
40
20
0
-20
-40
-60
0 2 4 6 8 10 12 14 16 18 20
Transient Time (Year)